Rare Met. (2021) 40(11):2993–3018
https://doi.org/10.1007/s12598-020-01696-8

RARE METALS

REVIEW

Interface materials for perovskite solar cells

Yi-Heng Zhang, Yuan Li*

Received: 17 August 2020 / Revised: 23 October 2020 / Accepted: 26 October 2020 / Published online: 3 June 2021

Abstract Perovskite solar cells exhibit great potential to become commercial photovoltaic technology due to their high power conversion efficiency, low cost, solution processability, and facile large-area device manufacture. Interface engineering plays a significant role to optimize device performance. For the anode in the inverted devices, this review introduces the progress on the modification of poly(3,4-ethylenedioxythiophene): poly(styrene sulfonate) including chemical structure alteration, physical doping, and solution treatment. We present the recent advances of dopant-free hole transport materials widely applied in mesoporous and conventional devices, outlining their innovation with novel molecular design concepts toward promising material properties, and device performance. For the cathode, various metal oxide and organic electron transport materials are covered and the different modification strategies and related mechanisms are highlighted. Most importantly, simple synthesis process, inexpensive raw materials and highly reproducible photovoltaic performance are the main consideration for the design of all the interface materials. Finally, an outlook and some suggestions regarding the future interface engineering are proposed based on the summary of the current development status and working mechanism of interface materials.

Keywords Perovskite solar cells; Interface; Hole transport materials; Electron transport materials; PEDOT:PSS

Y.-H. Zhang, Y. Li*
School of Materials Science and Engineering, South China University of Technology, Guangzhou 510641, China
e-mail: celiy@scut.edu.cn

1 Introduction

With the development of human civilization, the acquisition of energy has become an important topic for mankind. In recent years, with the climate and environmental problems brought about by the consumption of fossil energy, people have recognized the importance of researching and developing new green renewable energy to replace the fossil energy. Among the many green renewable energy sources, solar energy has the most development prospects because of its advantages such as wide distribution, no geographical restrictions and never running out [1].

At present, the silicon-based solar cells realize the most extensive commercial production. However, the cumbersome manufacturing process of silicon-based solar cells has become the key factors restricting their continued development. At the same time, it is a topic to fabricate a variety of inorganic multicomponent semiconductor thin-film solar cells. The most representative one of them is the device based on the III–V compound GaAs [2]. The power conversion efficiency (PCE) of GaAs-based solar cells realized 28%. In addition, the champion PCE of liquid-phase organic dye-sensitized solar cells was reported over 13% [3], but its PCE is difficult to be further improved. Besides, organic solar cells have attracted much attention because of their advantages such as low price, simple preparation process (such as spraying, squeegee) and ultra-thin large-area flexible devices. Recently, the breakthrough of organic solar cells based on non-fullerene acceptor achieves a high PCE of 18.0% [4, 5]. However, the PCE and stability of organic solar cells are relatively lower compared with those of inorganic solar cells.

In recent years, the perovskite solar cells (PSCs) have developed rapidly. In 2009, Tsutomu et al. discovered that

perovskite has the effect of absorbing sunlight and employed perovskite to form solar cells successfully preparing devices with PCE of 3.8% [6]. In the past 10 years, scientists have improved perovskite solar cell devices, making the PCE of PSCs exceed 25.2% [7]. At the same time, perovskite materials have shown strong absorption, high mobility, long carrier life, adjustable band gap and solution processability, so it has become one of the most attractive solar cell technologies. In the high-performance PSCs, the interface materials played a significant role in extracting and transporting carriers from the perovskite layer to the electrodes [8]. In this review, we mainly summarize the interface materials used in PSCs and discuss the effect of material structure on device performance.

2 Device structure of perovskite solar cells

In the field of solar cells, the perovskite material usually refers to the organic–inorganic hybrid perovskite metal halide ABX_3 material, and its structure is shown in Fig. 1a. A is generally a small-sized organic cation such as CH_3NH^{3+} (MA) and $CH_2(NH_2)_2$ (FA); B is generally a transition metal divalent ion, such as Pb^{2+}. X is a halogen ion (Cl^-, Br^-, I^-).

PSCs are mainly composed of a transparent conductive oxide (TCO) substrate, an electron transport layer (ETL), a perovskite layer, a hole transport layer (HTL) and a counter electrode (Au, Ag, Al or others). The mesoporous structure is the most important device structure in the early stage of the development of PSCs [9]. The composition is FTO/compact TiO_2 layer/mesoporous TiO_2 layer/perovskite layer/HTL/Au (Fig. 2a). The second category is a conventional planar heterojunction n–i–p structure (Fig. 2b) and an inverted planar heterojunction p–i–n structure (Fig. 2c). The structure of the conventional n–i–p device is FTO/compact TiO_2 layer/perovskite layer/HTL/Au or Ag, and that of the inverted p–i–n device is FTO or ITO/HTL/perovskite layer/ETL/Ag or Al. The fabrication process of the planar structure device is relatively simple, while the requirements for the film formation quality and interface of each layer are relatively high. Recently, PSC devices with 2D perovskite have been widely investigated to enhance their stability and performance through tuning the interface properties between the perovskite layer and the charge extraction layer [10–12]. Additionally, carbon-based PSCs are emerging as low-cost stable photovoltaics and have shown great potential [13].

When a photon with an energy greater than the perovskite bandgap is absorbed by the perovskite materials, the perovskite light-absorbing material is excited by light to generate excitons, and the excitons are separated inside the material and at the interface to form conduction band electrons and valence band holes. Then, electrons and holes are injected into the conduction band of the electron transport material (ETM) and the highest occupied molecular orbital (HOMO) of the hole transport material (HTM), respectively. Finally, the electrons and the holes were collected, thereby forming a complete cycle (Fig. 1b) [9].

3 Research progress of anode interface materials

The purpose of HTMs in PSCs is to extract and transport holes at the perovskite/HTM interface. The ideal HTMs should meet some general requirements to make it more efficient in PSCs. For example, the HTMs should have a compatible HOMO energy level with the perovskite valence band energy level, good stability and superb hole mobility. Besides, the low cost and convenient synthesis

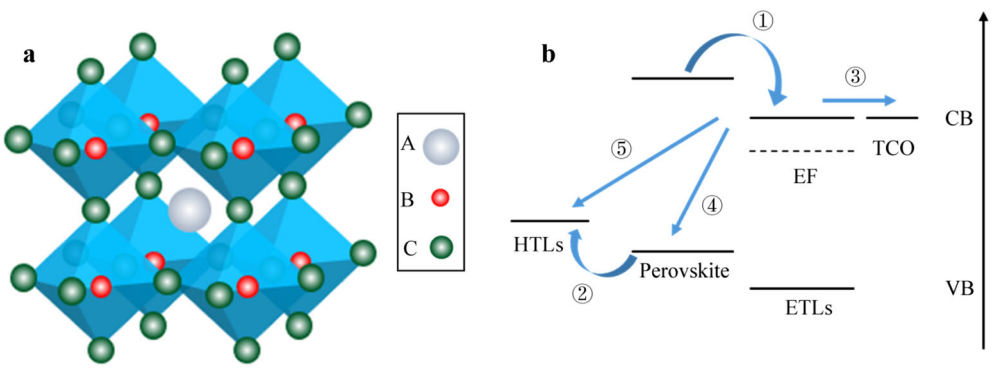

Fig. 1 **a** Crystal structure of cubic perovskite with generic chemical formula ABX_3. **b** Schematic representation of charge transfer processes in perovskite solar cells: Route ①—electron injection, Route ②—hole injection, Route ③—electron transport and collection, Route ④—charge recombination in interface between ETLs and perovskite, Route ⑤—charge recombination between electrons ETLs and holes in HTLs. Reproduced with permission from Ref. [9]. Copyright 2016 Royal Society of Chemistry

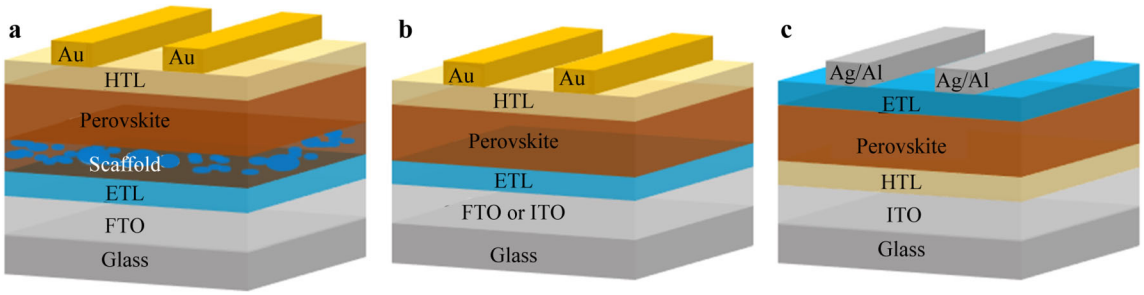

Fig. 2 Most common PSC device architectures: **a** mesoporous n–i–p structure, **b** conventional planar n–i–p structure and **c** inverted planar p–i–n structure

process of HTMs can make it possible to prepare commercially. Recently, many HTMs have been developed and incorporated for high-efficiency PSCs. Owing to the length of the article, inorganic hole transport materials will not be introduced in details. However, organic HTMs can basically be divided into three categories: conductive polymers, small-molecule HTMs and organometallic complexes. Herein, this review will focus on the organic conductive polymers and organic small-molecule HTMs.

3.1 Conductive polymers—PEDOT-based hole transport materials

Poly(3,4-ethylenedioxythiophene) (PEDOT) is a thiophene-based conductive polymer with the typical properties of doped conductive materials [14]. In recent years, PEDOT has received extensive attention in the fields of organic optoelectronics [15], bioelectronics [16] and electrochemistry [17, 18], owing to the advantages of high transparency, remarkable thermal stability, tunable conductivity and good film forming [19]. In view of the molecular structure of PEDOT, the introduction of ethylenedioxy at the 4-position of the thiophene ring not only makes the polymer chain more regular and orderly, but also increases the density of the electron cloud on the thiophene ring [14]. Meanwhile, the oxidative doping potential of PEDOT also decreases, and its conductive doping state is tending toward stability [20, 21]. However, the main chain of PEDOT with strong π–π stacking is a sort of rigid conjugated structure, resulting in insolubility and infusibility under eigenstate [22]. This makes further processing difficult and limits the applications of PEDOT.

In order to solve the problem of poor solubility in the PEDOT eigenstate, Bayer creatively used poly(styrene sulfonate) (PSS) to disperse PEDOT [23]. Generally, a stable black-blue PEDOT:PSS suspension is obtained by mixing a certain proportion of 3,4-ethylenedioxythiophene (EDOT) and PSS under acidic conditions with an oxidizing agent such as ammonium persulfate. In this system, PSS acted as a dispersant, and its hydrophilic group allowed insoluble PEDOT to be stably dispersed in aqueous solution [21–23]. Additionally, PSS was also an anionic dopant that maintains charge balance in the PEDOT backbone forming p-type doped PEDOT:PSS [24, 25]. Moreover, the PSS also plays as a template which allows the linear PEDOT to be arranged along with a linear conformation [26]. It was recognized that the introduction of PSS with long straight chain and no double-bond structure endowed the PEDOT:PSS aqueous solution with low cost, easy processing and high mechanical flexibility, which provided the basis for being widely used in light-emitting diodes [27, 28], organic solar cells [29–31] and supercapacitors [32, 33]. Especially in the device structure of inverted PSCs, PEDOT:PSS was generally used as an HTM, offering intrinsic higher conductivity and lower tendency to crystallize compared with their small-molecule analogues [34]. Furthermore, the performance of PSCs with PEDOT:PSS has made impressive progress with maximum PCEs exceeding 22% for state-of-the-art devices [35–39]. However, there were still some limitations in the application process with the addition of insulators because the addition of PSS led to a poor conductivity uniformity.

Based on the discussion above, this review mainly discusses the physical and modification of PEDOT:PSS that could effectively improve the performance of PSCs.

It was generally believed that the significant improvement of PEDOT:PSS conductivity was very important for its application as the transparent layer of optoelectronic devices [40]. The conductivity enhancement of PEDOT:PSS was discovered in 2002 by Kim et al. [41] with the addition of organic solvents such as dimethyl sulfoxide (DMSO), dimethyl formamide (DMF) or tetrahydrofuran (THF). Since then, many methods have been reported to tune the conductivity of PEDOT:PSS [42–48]. Shi et al. [19] further summarized that efficient approaches to improve the electrical conductivity of PEDOT:PSS are thermal/light/organic solvent/surfactant/salt solution/zwitterion/acid or alkali treatment and pH value influences.

Though the electrical conductivity of PEDOT:PSS could be efficiently enhanced by a couple of methods, it was still

a big challenge to clearly understand the intrinsic conductivity mechanism at this stage. Up to now, some researchers have proposed different mechanisms to explain the effect of the treatments on the structure of PEDOT:PSS. In order to fully explore the influence of the molecular weight of additives on the conductivity of PEDOT:PSS, Mengistie et al. [49] selected polyethylene glycol (PEG) and ethylene glycol (EG) with different concentrations and molecular weights, respectively. This work revealed that the depletion of PSS on the membrane surface would cause the conformation of PEDOT to change from a coiled structure to a linear/extended coil structure, which was consistent with the atomic force microscope (AFM) phase diagram. The ionic interaction between PEDOT and PSS with the addition of PEG or EG would be produced owing to forming hydrogen bonding with both PSS^- and PSSH, which resulted in better phase separation between PEDOT and PSS, linear arrangement of PEDOT chains and larger or more aggregated PEDOT chains on the film surface. Therefore, due to the linear structure, larger grain size and lower intergrain hopping, the electrical conductivity of PEDOT-rich chains was greatly improved. Before that, Ouyang et al. [50] found that the chain interaction between the PEDOT chains was enhanced after EG treatment, which caused the water-soluble PEDOT:PSS became insoluble. The study further found that the increase in conductivity was related to the two or more pole groups in the molecule, which would promote the change of the resonance structure of the PEDOT chain from a benzoid to a quinoid structure confirmed by Raman spectroscopic.

Chu et al. proposed a simple and efficient film treatment method, in which they used methanol with stronger hydrophilicity and higher dielectric constant to treat PEDOT:PSS film [51]. The conductivity could be improved by immersing the film in methanol, dropping a small amount of methanol on the film or a combination of the two methods for PEDOT:PSS film treatment, while mixing methanol in the PEDOT:PSS aqueous solution had almost no effect on the conductivity. For single-layer PEDOT:PSS film, the conductivity was increased from 0.3 to 1362 $S{\cdot}cm^{-1}$, while maintaining high transmittance. Rivnay's group [52] employed synchrotron radiation and resonant soft X-ray scattering to investigate the multi-scale microstructure of PEDOT:PSS films in the premise of PEDOT:PSS films modified with varying amounts of co-solvent. In this work, the multi-scale morphological changes caused by the addition of commonly used co-solvents and successfully built the structure–characteristic relationship describing the blended conductivity in the prototype conducting polymers. Gelbwaser-Klimovsky et al. [53] proposed that the structure in the PEDOT:PSS film was very disordered, which would make a great contribution to the optical and electronic properties. Additionally, Reyes-Reyes et al. [54] conceived a new doping scheme by using dimethyl sulfate in the PEDOT:PSS dispersion. After this treatment, the conductivity of the PEDOT:PSS film was 1880 times higher than that of the original PEDOT:PSS. Attractively, DMS enhanced the doping level in the PEDOT chains replacing some PSS units with SO_4^{2-} in the film, and this enhancement was mainly produced with a very low pH of the solution. In addition, Li et al. [55] introduced non-toxic, low-cost and water-soluble carbon nanodots (CNDs) into PEDOT:PSS and successfully prepared PEDOT:PSS:CNDs. The PEDOT:PSS doped with CNDs effectively removed the insulating parts. Therefore, the conductivity and hole extraction capability of PEDOT:PSS:CNDs were significantly improved, compared with the original PEDOT:PSS.

In general, despite the growing number of reports relating to the conductivity enhancement mechanism of PEDOT:PSS, it was difficult to put forward an original model to guide the modification design of PEDOT, limited by the characterization technique. Also, there were difficulties in understanding the effect of the treatments on the structure of PEDOT:PSS. It was believed that further efforts were needed in order to fully understand the law of conductivity enhancement to create more superior modified PEDOT:PSS for PSCs.

3.1.1 Modification via doping

The p–i–n inverted plane PSCs with PEDOT:PSS as the HTL was a popular research topic [56, 57]. Recent studies have achieved better device performance through the modification of PEDOT:PSS. Liu et al. [58] introduced 2,3,5,6-tetrafluoro-7,7,8,8-tetracyanoquinodimethane (F4-TCNQ) dopant into PEDOT:PSS as HTL of PSC devices for the first time. The doped PEDOT:PSS film showed enhanced conductivity and achieved lower work function, and the recombination of charge carriers decreased, resulting in short-circuit current (J_{SC}) and open-circuit voltage (V_{OC}) increased simultaneously. Compared with the reference devices, the optimized devices could realize a significant increase in PCE from 13.30% to 17.22%. Huang et al. [59] fabricated DMSO-doped PEDOT:PSS, which improved absorption, morphology, crystallinity, conductivity and inhibited interface reorganization. Herein, the PCE of the PSC devices with SMSO-doped PEDOT:PSS as the HTL increased by 37%. Besides, Thomas et al. [60] studied the changes in the morphology and nanostructure properties of PEDOT:PSS after adding two commonly used co-solvents DMSO and EG. Wang et al. [61] developed an inverted silicon nanopyramid surface structure by sequentially processing NaOH and $HF/CH_3COOH/HNO_3$ solutions to Si nanowires textured Si wafers. Owing to the higher junction and contact quality, the PCE of the device

was enhanced to 9.6%. Kim et al. [62] employed polyethyleneimine (PEI) to modify PEDOT:PSS (PH1000) to adjust the work function and applied it to the ITO/PEDOT:PSS/$CH_3NH_3PbI_3$/PCBM layer. Furthermore, the PEI treatment of PH1000 reduced the work function from 5.1 to 3.97 eV.

Li's group fabricated highly efficient planar heterojunction PSCs with dopamine (DA) semiquinone radical modified poly(3,4-ethylenedioxythiophene) polystyrene sulfonate (PEDOT:PSS) (DA-PEDOT:PSS) as an HTL [25, 63]. Compared with PEDOT:PSS, DA-PEDOT:PSS had a higher radical content and a larger perovskite charge extraction capacity for HTL (Fig. 3a-c). In addition, DA doping also improved the work function of PEDOT:PSS and increased the crystallinity of the perovskite film. In addition, the amino groups and hydroxyl groups in DA could interact with the uncoordinated Pb atoms on the surface of perovskite layer to reduce the charge recombination and improve the charge extraction. Furthermore, Dong et al. [64] introduced hydroxymethyl (–MeOH) functional group into ethylenedioxythiophene (EDOT) to form a hydroxymethylated 3,4-ethylenedioxythiophene (EDOT-MeOH) monomers and to further polymerize them to water-soluble poly(hydroxymethylated-3,4-ethylenedioxythiophene):polystyrene sulfonate (PEDOT-MeOH:PSS) to improve PEDOT:PSS with the electronic, structural and surface morphological properties. Then, this group found that increasing the amount of iron trioxide oxidant would simultaneously increase the conductivity and work function of the PEDOT-MeOH:PSS film, and by adding EG could effectively enhance the conductivity of PEDOT-MeOH:PSS film, because hydrogen bonding between EG and -MeOH groups on PEDOT-MeOH facilitated the structural change of PEDOT-MeOH backbone from the benzoid to quinoid structure and the phase segregation of PEDOT-MeOH and PSS domains.

In order to reduce the influence of the interface barrier, Zhang et al. [65] treated the surface of PEDOT:PSS with hydroquinone (HQ), which lowered the hole transport barrier at the interface, thereby reducing the interface resistance. The crystal size of the perovskite film grown on the PEDOT:PSS after the HQ spin coating process was larger than the crystal size of the perovskite film on the PEDOT:PSS without the HQ process. These results indicated that HQ-doped PEDOT:PSS improved the crystallinity and crystal quality of the perovskite film grown on it. Subsequently, this team changed the content (wt%) of HQ and isopropyl alcohol (IPA) and found that when the ratio was 0.5 wt%, PCE achieved the maximum value of 14.65%, J_{SC} was 27.07 mA·cm^{-2}, V_{OC} was 0.737 V, and FF was 73.44%. Recently, adding dopants to PEDOT:PSS has also become an effective strategy to improve the PCE of PSCs. Zhao et al. [66] systematically studied the effects of 3-(cyclohexylamino)-2-hydroxy-1-propanesulfonic acid (CAPSO) doping PEDOT:PSS and perovskite film performance in PSCs. CAPSO zwitterions could significantly increase the conductivity and improve the wettability of the PEDOT:PSS layer and the polar perovskite solution, thereby increasing the PCE of the $CH_3NH_3PbI_3$-based device. When the optimal doping concentration of CAPSO was 15 mg·ml^{-1}, the conductivity measurement showed that the conductivity of the PEDOT:PSS film doped with CAPSO has increased by nearly three orders of magnitude, which was beneficial for effective charge extraction. Above all, using this method to fabricate high-efficiency PSCs, compared with the original PEDOT:PSS HTL-based reference device, the efficiency of the device containing CAPSO-doped PEDOT:PSS HTL increased by more than 40%. In addition, Xu et al. [67] introduced CuSCN to modify PEDOT:PSS to fabricate PEDOT:PSS-CuSCN composite layer as HTL which could significantly enhance PCE and improve the long-term stability of inverted PSC. PEDOT:PSS-CuSCN composite film has lower acidity and higher work function, which is beneficial to the improvement and stability of charge extraction efficiency. At the same time, the HTL modified by CuSCN could also promote the crystallization of the perovskite film, resulting in an increase in the grain size and a decrease in the boundary. Finally, the PEDOT:PSS-CuSCN-based PSCs achieved

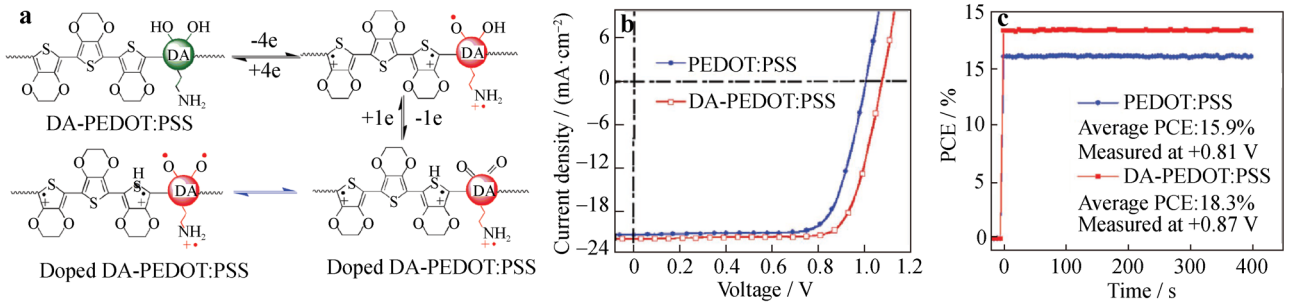

Fig. 3 **a** DA-PEDOT:PSS:DA semiquinone radicals; **b** photovoltaic performance of PSCs with PEDOT:PSS and DA-PEDOT:PSS; **c** long-term stability of unencapsulated PSCs. Reproduced with permission from Ref. [63]. Copyright 2018 John Wiley and Sons

higher PCEs of 15.3%, which is 16% higher than that of the control device.

3.1.2 Modification via changing chemical structure

Although PEDOT:PSS has been developing for nearly 30 years acting as one of the most famous traditional HTMs in photovoltaic devices, in fact, there still existed a lot of drawbacks for PEDOT:PSS due to its relatively low work function (4.8–5.1 eV). Besides, the ultra-high molecular weight and linear structure of the dopant PSS induced a partial bonding of PSS with PEDOT, greatly reducing the structural and electrical homogeneity of PEDOT:PSS system. Hence, it was necessary to hunt for the novel dispersants of PEDOT in order to optimize the performance of PSCs.

Li et al. grafted alkali lignin (AL) with sulfonated formaldehyde acetone condensate (SAF) to obtain sulfonated formaldehyde acetone–lignin (GSL). PEDOT:GSL was used as an HTL for PSCs for the first time, and its PCE was higher than that of PEDOT:PSS devices (Fig. 4) [68–70]. Furthermore, the PEDOT:LS-based PSC showed a higher long-term stability compared with the PEDOT:PSS reference device due to the excellent waterproofness of hole extraction layer [71]. In this article, the covalent bonding between LS and PEDOT during the oxidation polymerization process could improve the homogeneity of PEDOT:LS, and the cross-linking between LSs with the heating process could result in a dense film with excellent waterproofness. More importantly, the unencapsulated PEDOT:LS-based devices showed higher long-term stability not only in N_2 but also in air than those of the unencapsulated PEDOT:PSS-based devices. After 158 h, the PEDOT:LS-based device retained more than 96.1% of its original PCE, whereas the PEDOT:PSS-based device retained about 90.7% of its original PCEs. Furthermore, Huang et al. [72] introduced DA into PEDOT:LS to adjust the work function. This work pointed out that the alkalinity of DA would reduce the acidity and hydrophilicity of PEDOT:LS, and the inherent cross-linking between LS, DA and PEDOT might produce water resistance, which was important for enhancing the durability of PSC devices (Fig. 5a–c). Additionally, the V_{OC} value of PSCs based on PDA:PEDOT:LS was 1.02 V; therefore, PCE of the devices was enhanced. At the same time, the acidity of PDA:PEDOT:LS was reduced, so the devices realized excellent water resistance and lower hydrophilicity.

Yu et al. [73, 74] employed the second-generation water-reducing agent sulfoacetone formaldehyde condensate (SAF) instead of PSS to fabricate a new HTM (PEDOT:SAF). PEDOT:SAF had lower acidity and higher work function, which could reduce the UV degradation of the perovskite layer. In addition, compared with commercial PEDOT:PSS, PEDOT:SAF was easy to be prepared and low in cost. Besides, it had great dispersion stability in aqueous solutions, good film-forming properties and higher electrical conductivity. Therefore, PSCs with the new PEDOT:SAF as the HEL have achieved excellent performance, with a high PCE of 14.05%. Especially in terms of equipment stability, after nearly a month of storage, PSCs based on PEDOT:SAF retained 83.2% of PCE, while PSCs based on PEDOT:PSS retained only 57.4% of its initial value (Fig. 5d–f). Besides, Li et al. reported a new water-

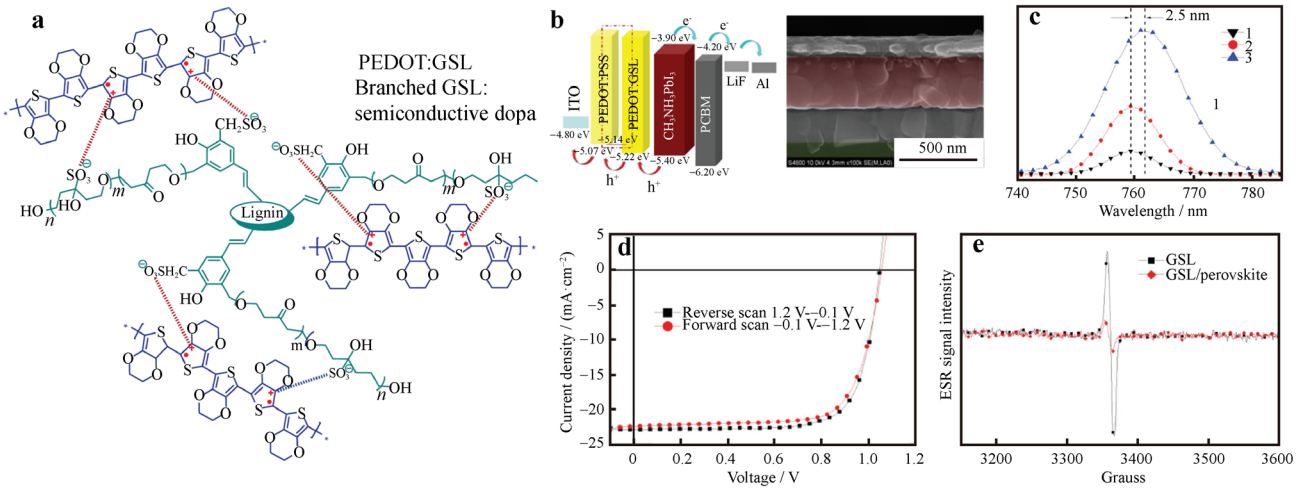

Fig. 4 **a** Schematic of PEDOT:GSLs; **b** energy level diagram of PSC and cross-sectional SEM image; **c** steady-state PL spectroscopy of 1 ITO/PEDOT:PSS/PEDOT:GSL/perovskite, 2 ITO/PEDOT:GSL/perovskite and 3 ITO/PEDOT:PSS/perovskite; **d** current density–voltage characteristics of PSC with bilayer HTLs; **e** electron spin resonance spectra of GSL and GSL/perovskite. Reproduced with permission from Ref. [68]. Copyright 2017 John Wiley and Sons

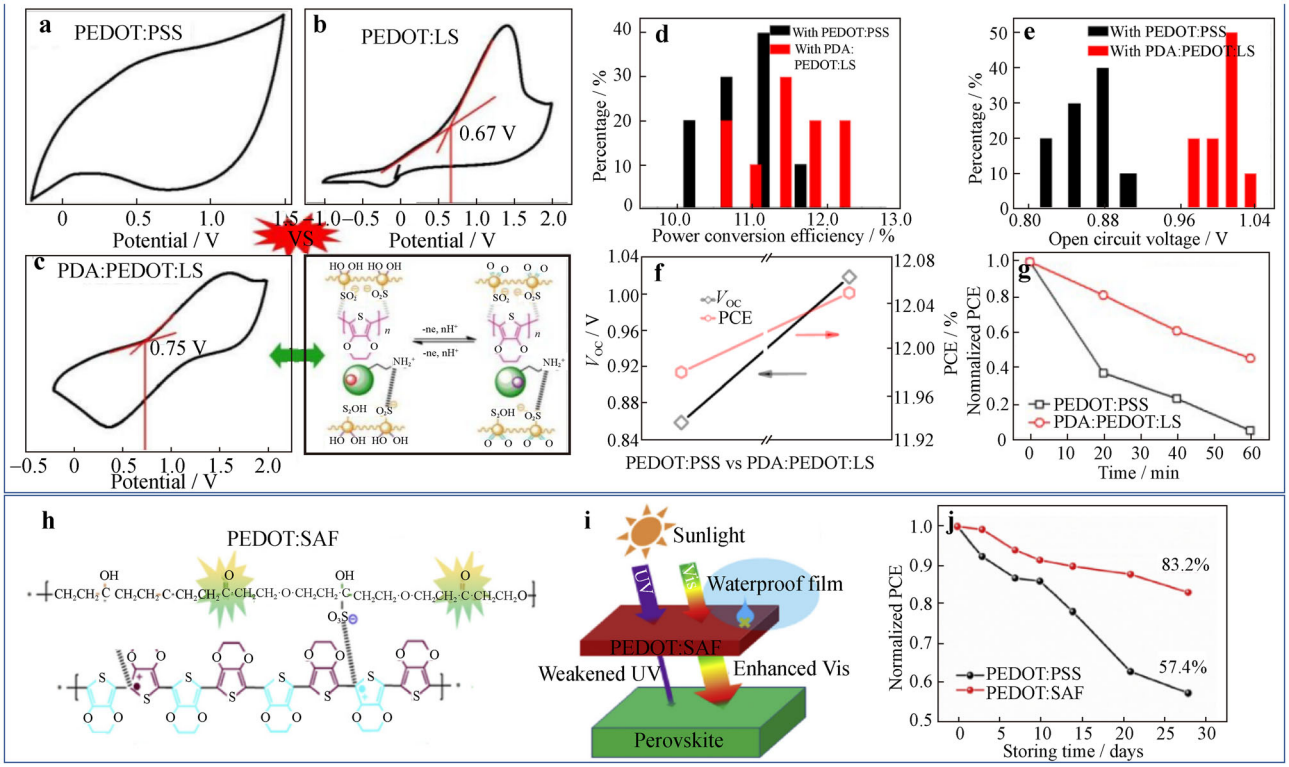

Fig. 5 Cyclic voltammograms of sample films with 0.1 mol·L^{-1} Bu_4NPF_6 in CH_2Cl_2 solution: **a** PEDOT:PSS; **b** PEDOT:LS; **c** PDA:PEDOT:LS, and the mechanism for the change of the work function for PDA:PEDOT:LS **d** PCE and **e** V_{OC}; **f** change trend for V_{OC} and PCE of champion devices; **g** stability characteristics of PSCs with PEDOT:PSS and PDA:PEDOT:LS as HTL. Reproduced with permission from Ref. [72]. Copyright 2017 Royal Society of Chemistry. **h** Chemical structure of PEDOT:SAF; **i** UV absorbing effect of HEL with PEDOT:SAF toward perovskite layer; **j** stability characteristics of PSCs with PEDOT:PSS and PEDOT:SAF as HEL. Reproduced with permission from Ref. [73]. Copyright 2017 Elsevier

soluble sulfobutylated phenol formaldehyde resin with flexible alkyl sulfonic acid groups, which was served as semiconductive dopant because of the stable oxidation state with radical [70].

Li et al. [75] fabricated PEDOT:MNSF by a one-step oxidation method using a branched dispersant, methylnaphthalene sulfonate formaldehyde condensate (MNSF). Compared with PEDOT:PSS, PEDOT:MNSF had very low electrical conductivity, but it had the advantages of high work function and good electrical conductivity uniformity (Fig. 6). It exhibited high performance in inverted $CH_3NH_3PbI_xCl_{3-x}$-based PSCs. This work pointed out that the dopant PSS with the ultra-high molecular weight and the linear structure was only partially combined with PEDOT, which greatly reduced the structural uniformity of the PEDOT:PSS film, verified by X-ray photoelectron spectroscopy (XPS). Additionally, The PEDOT:PSS and PEDOT:MNSF were compared by phase separation experiments and conductive atomic force microscopy (c-AFM). The results proved that the excessive and insulated PSS in PEDOT:PSS had a great influence on the uniformity of the film's conductivity. There was still high performance for PEDOT:MNSF with very low conductivity because of good structural uniformity and conductivity uniformity. Based on the above, the successful applications in exploring novel dispersant of PEDOT encouraged us to study additional types of dispersants and its further application in organic electronics.

3.2 Small-molecule hole transport materials

In 2012, Kim et al. [76] used solid organic HTM 2,2′,7,7′-tetrakis-(N,N-di-4-methoxyphenyl amino)-9,9′-spirobifluorene (Spiro-OMeTAD) to replace liquid as the electrolyte. The all-solid-state perovskite solar cell was manufactured for the first time, and its cross-sectional SEM image is shown in Fig. 7. The use of solid HTMs increased the efficiency of PSCs to 9.8%, while avoiding the decomposition of light-absorbing materials in polar solvents and improving the stability of the cells. Spiro-OMeTAD has since become the most representative small-molecule HTM (SM-HTM) in PSCs. However, Spiro-OMeTAD also had many shortcomings, such as complex synthesis process, difficult passivation and harsh reaction conditions leading to expensive cost, and low hole mobility, relying on dopants such as

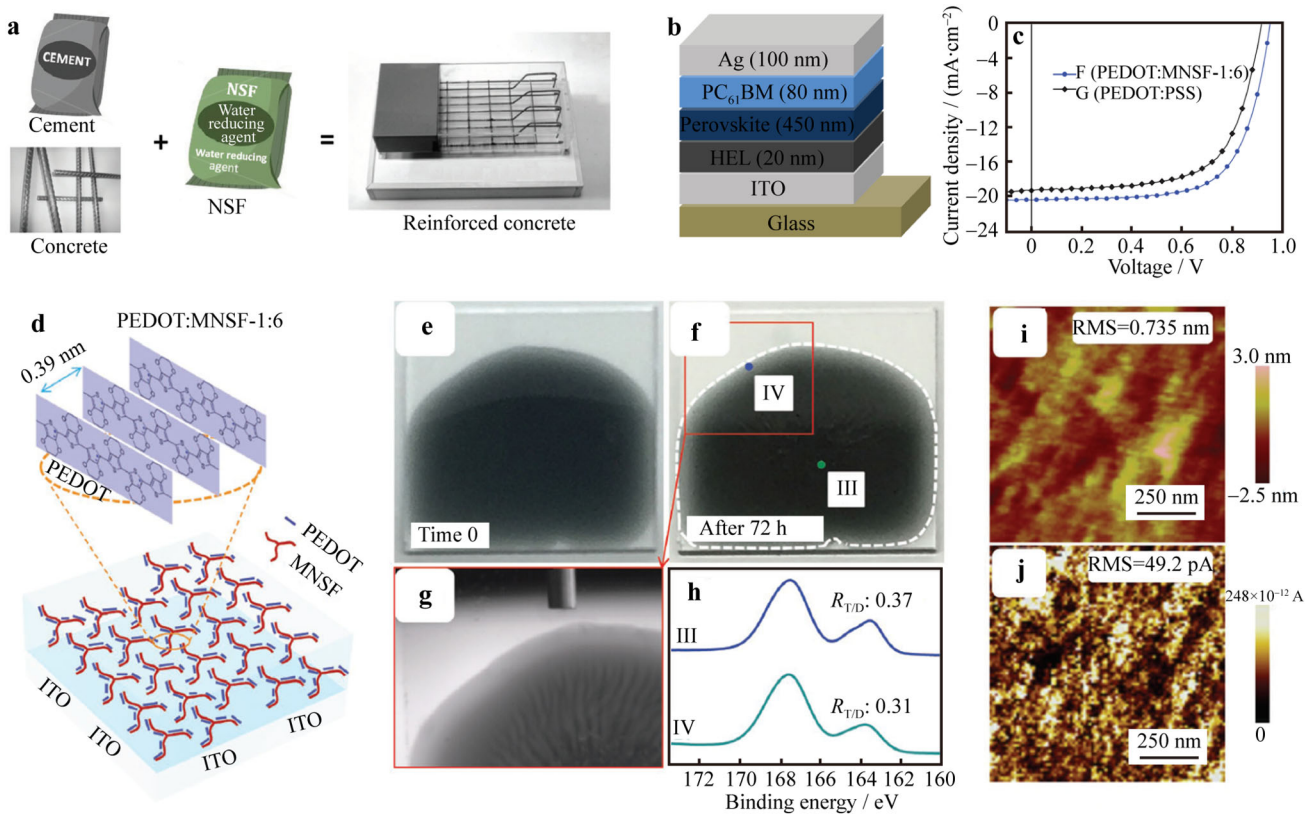

Fig. 6 **a** Schematic diagram of naphthalene sulfonate formaldehyde condensate (NSF) superplasticizer participated in reinforced concrete; **b** device architecture of inverted PSCs with PEDOT:MNSF-1:6; **c** current–voltage curves of inverted PSC devices F and G; **d** schematic of molecular packing and arrangement of PEDOT:MNSF-1:6; diagrams of samples in DMSO:H_2O (*V*/*V* of 1:4) drying in air atmosphere at room temperature (photographed using a JC2000C1 static contact angle instrument): **e** image of pristine samples drop cast onto glass substrates and **f** image of completely dried sample films; **g** image of border of completely dried sample films; **h** XPS S2p spectra acquired at positions III and IV in **f** ($R_{T/D}$ meaning PEDOT to dopant mass ratios); c-AFM images of sample films spin-coated on ITO after annealing at 120 °C for 15 min: **i** topography and **j** corresponding current map of PEDOT:MNSF-1:6 film, with bias voltage of 1 V. Reproduced with permission from Ref. [75]. Copyright 2017 John Wiley and Sons

bistrifluoromethanesulfonimide lithium salt (Li-TFSI) to increase its hole migration rate. Importantly, devices added with dopants tend to absorb moisture in the atmosphere and cause performance degradation. These shortcomings restricted its large-scale application in PSCs. Therefore, it was of great significance to develop novel SM-HTMs with simple synthesis, low cost and high hole mobility to replace Spiro-OMeTAD.

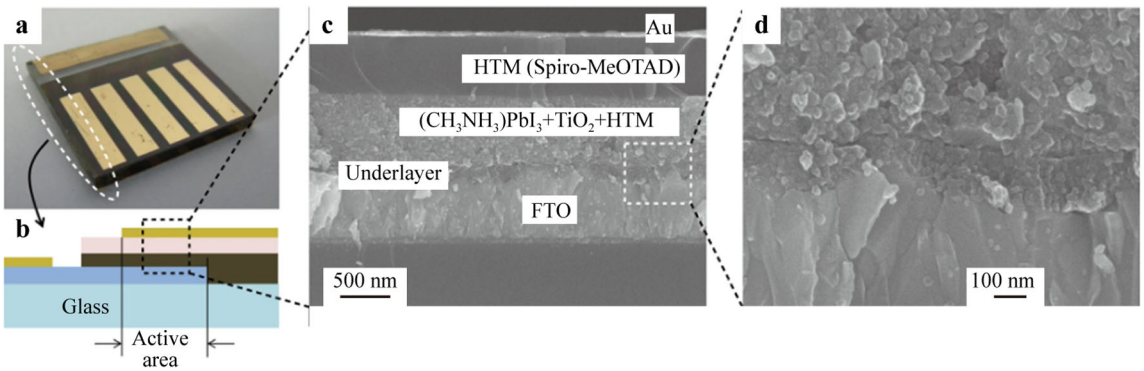

Fig. 7 Solid-state device and its cross-sectional meso-structure: **a** real solid-state device; **b** cross-sectional structure of device; **c** cross-sectional SEM image of device; **d** active layer–underlayer–FTO interfacial junction structure. Reproduced with permission from Ref. [76], Copyright 2012 Springer Nature

Table 1 Photovoltaic parameters of PSCs with small molecule hole transport materials

HTM	Device structure	Hole mobility/ ($cm^2 \cdot V^{-1} \cdot s^{-1}$)	HOMO/ eV	V_{OC}/ V	J_{SC}/ ($mA \cdot cm^{-2}$)	FF/%	PCE/ %	Refs.
DTB-FL	FTO/SnO_2/perovskite/HTM/MoO_3/Ag	3.94×10^{-3}	− 5.47	1.14	23.80	79.10	21.50	[8]
TQ2	FTO/cp-TiO_2/mp-TiO_2/perovskite/HTM/Au	2.29×10^{-4}	− 5.30	1.12	22.09	77.67	19.62	[77]
Z30	FTO/cp-TiO_2/mp-TiO_2/perovskite/HTM/Au	6.70×10^{-5}	− 5.27	1.11	23.53	73.00	19.17	[78]
YN2	FTO/cp-TiO_2/mp-TiO_2/perovskite/HTM/Au	9.65×10^{-4}	− 5.40	1.11	23.15	75.00	19.27	[79]
YN3	FTO/cp-TiO_2/mp-TiO_2/perovskite/HTM/Au	2.25×10^{-4}	− 5.31	1.12	22.43	75.00	18.84	[80]
MPA-BTTI	Ag/C_{60} + BCP/perovskite/HTM/ITO	2.20×10^{-4}	− 5.32	1.12	23.23	81.40	21.17	[81]
TPA-ANT-TPA	FTO/cp-TiO_2/mp-TiO_2/perovskite/HTM/Ag	2.60×10^{-4}	− 5.41	1.03	21.07	79.60	17.50	[82]
TPA-BPFN-TPA	FTO/cp-TiO_2/mp-TiO_2/perovskite/HTM/Ag	2.90×10^{-4}	− 5.47	1.04	22.70	78.00	18.40	[83]
DTP-C6Th	Au/HTM/perovskite/SnO_2/C_{60}-SAM/FTO	4.18×10^{-4}	− 4.87	1.16	22.76	79.90	21.04	[84]
DFH	Ag/C_{60} + BCP/perovskite/HTM/ITO	$\sim 1.00 \times 10^{-3}$	− 5.40	1.09	22.70	83.00	20.06	[85]
TPE-S	Ag/ZnO/PCBM/perovskite/HTM/ITO	1.20×10^{-5}	− 5.29	1.13	23.30	79.70	21.00	[86]
TXTX-OMeDPA	FTO/TiO_2/FA perovskite/HTM/Au	9.50×10^{-4}	− 4.79	1.15	24.78	78.00	22.20	[87]
K-DHP-1	FTO/cp-TiO_2/mp-TiO_2/perovskite/HTM/Au	2.98×10^{-4}	− 5.33	1.09	23.96	78.60	20.52	[88]

Because of the advantages of simple synthesis, easy purification, low production cost, diversity of molecular structure, solution processing and compatible with flexible equipment, SM-HTMs had become the focus of researchers. Furthermore, triphenylamine (TPA)/diphenylamine (DPA)-based compounds are the most popular SM-HTMs in PSCs. In this review, the recent researches on SM-HTMs for high-efficiency PSCs are introduced. All photovoltaic parameters of SM-HTM based on PSCs are listed in Table 1 [8, 77–88], and their chemical structures are shown in Fig. 8. In order to pursue cost-effective and excellent performance HTMs, various groups have designed novel small molecule-based materials with different concepts.

In order to adjust HOMO levels, Zhang et al. [77] synthesized a series of D-A-D HTMs with quinoxaline as the core. Among these materials, TQ2 has an appropriate HOMO level, and the champion PCE of PSCs with TQ2 was 19.62%, which surpassed that of devices with Spiro-OMeTAD under the same conditions. Through photoluminescence quenching and electrical measurements, it was found that the structural change of the quinoxaline core substituent from phenyl (TQ1) to thienyl (TQ2) not only shortened the hole extraction time (16.6 vs. 3.4 ns), but also improved hole mobility (9.45×10^{-5} $cm^2 \cdot V^{-1} \cdot s^{-1}$ vs. 2.29×10^{-4} $cm^2 \cdot V^{-1} \cdot s^{-1}$) and electrical conductivity (6.58×10^{-5} $S \cdot cm^{-1}$ vs. 9.19×10^{-4} $S \cdot cm^{-1}$). Single-crystal analysis showed that the thiophene substituent in TQ2 would cause strong intermolecular S–S and S–π interactions, thereby reducing the intermolecular distance and increasing the hole hopping channel, which was beneficial to the charge transport in the HTL. In a large-area device of 1.02 cm^2, TQ2 was further preliminary scaled up and tested, and the results showed an efficiency of 18.50%. Besides, Zhang et al. [78] synthesized a series of HTMs based on phenothiazine core, and devices with Z30 as the HTM have achieved a high PCE of 19.17%. This was because Z30 had good solubility, sufficiently high hole mobility and an appropriate HOMO level. More importantly, compared to Z28 and Z29, the Z30-based devices aging for 1008 h in the dark at 40% relative humidity in the ambient air showed better performance when immersed in continuous sunlight for 600 h without packaging stability. Before that, Xue et al. [89] fabricated a series of phenol core HTMs with ultra-wide bandgap and excellent film-forming properties called TCP-OH and TCP-OC_8 (Fig. 9). Compared with TCP-OC_8, TCP-OH showed a higher glass

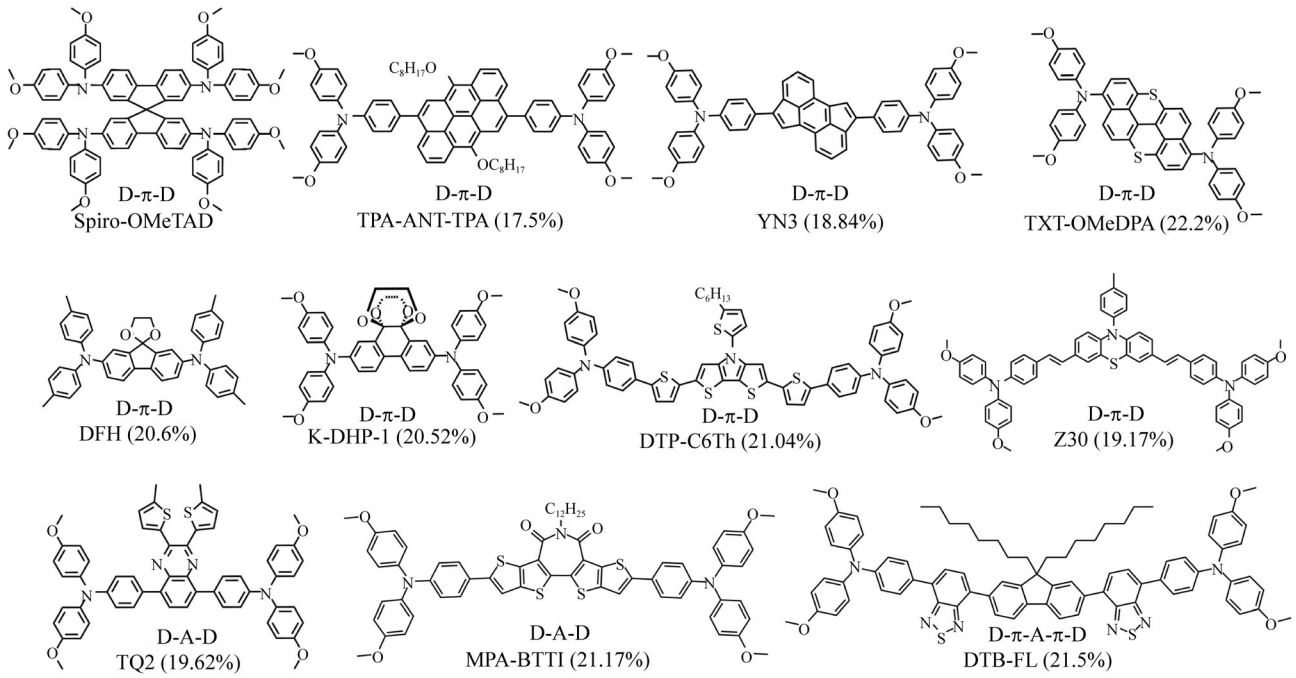

Fig. 8 Molecular structures of small-molecule hole transport materials

transition temperature, better matching band arrangement and higher hole mobility. The synthesis route of TCP-OH and TCP-OC_8 was very simple, and they are one of the first small molecules without methoxy groups. The photovoltaic performances of TCP-OH-based devices have achieved the highest record at the time. Recently, Li et al. proposed a new dopant-free HTM named DTB-FL with a D–A–π–A–D molecular design [8]. The donor (D) unit based on 4-methoxy-N-(4-methoxyphenyl)-N-phenylaniline has been considered as the efficient terminal group in HTM. The acceptor (A) unit based on benzothiadiazole features structural planarity, benefiting to the enhanced intermolecular stacking. A 9,9-dialkylfluorene unit with weak electron-donating strength was selected as the middle π-bridge; such modification not only could ensure good solubility and film formation properties of the molecules, electronically, but also extended the overall π-conjugation length of the molecule and deepened its HOMO energy level. Meanwhile, the 2,7-substitution on 9,9-dialkylfluorene core contributed to a more linear conjugated structure of HTM, which might feature better material properties in contrast to the twisted one created by the 3,6-substitution. This work showed that the PSCs based on undoped DTB-FL HTM were outperformed those based on DT-BT and doped Spiro HTMs exhibited a champion PCE of 21.5% with negligible photocurrent hysteresis, which was among the highest performance for MA-free PSCs based on dopant-free molecular HTM.

Xu et al. [79] synthesized a new HTM named YN2 which contained TPA as the donor and thieno[3,4-b]pyrazine (TP) unit as the acceptor. Compared with YN1 whose acceptor is benzothiadiazole (BT) unit, YN2 showed better hole extraction ability, higher hole mobility and smoother interface. The PCE of the PSC devices with YN2 as the HTM achieved 19.27%, which was better than the PCE of the PSCs made with Spiro-OMeTAD (17.80%), while the PCE of the PSCs with YN1 as the HTM was much lower at 16.03%. This result indicated that the photoelectric performance of D–A–D HTM could be fine-tuned by introducing various electron-withdrawing groups. In addition, This team fabricated a new HTM named YN3 with cyclopenta[hi]aceanthrylene as the acceptor [80]. They hoped to employ cyclopenta[hi]aceanthrylene's large planar aromatic π-conjugation structure to form π–π interactions between molecules, thereby improving the ordered morphology of the solid film. The $(FAPbI_3)_{0.85}(MAPbBr_3)_{0.15}$ PSC devices based on YN3 as a dopant-free HTM had a very impressive PCE of 18.84% with a low hysteresis, which was higher than the doped Spiro-OMeTAD-based reference device (18.41%) under the same working conditions. The PCE of the $CsPbI_2Br$ solar cell based on YN3 HTM was 12.05%, exceeding the cell with a PCE of 11.51% based on the reference Spiro-OMeTAD.

In the molecular design engineering of SM-HTMs, the electron acceptor unit was also used as the core. Guo et al. designed and synthesized two SM-HTMs, called MPA-BTI and MPA-BTTI, using imide-functionalized fusion units as

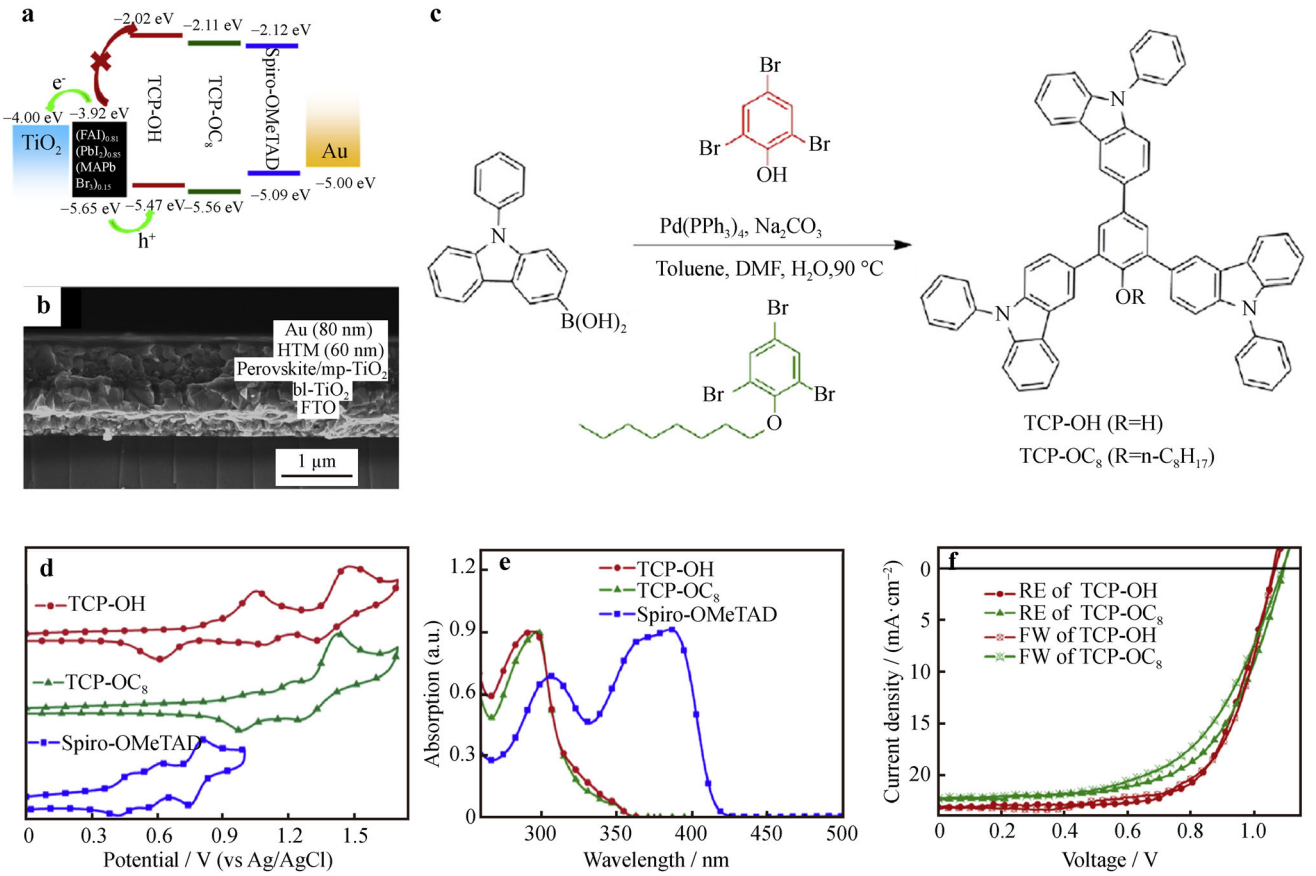

Fig. 9 **a** Diagram of energy level for each layer in PSC device; **b** cross-sectional SEM image of a representative device; **c** synthetic route of TCP-OH and TCP-OC8; **d** cyclic voltammograms of TCP-OH, TCP-OC_8 and Spiro-OMeTAD in dichloromethane solution; **e** UV–Vis absorption spectra of TCP-OH, TCP-OC_8 and Spiro-OMeTAD in dichloromethane; **f** *J*–*V* curves of champion devices. Reproduced with permission from Ref. [89]. Copyright 2017 Elsevier

the core (Fig. 10) [81]. In this molecule, the imide-based fusion thiophene unit was the acceptor unit, and TPA units were the donors. The high planarity of the cores could achieve great intermolecular π–π stacking, which facilitated charge transfer. At the same time, due to insufficient coordination between the S atom of HTM and the Pb^{2+} of the perovskite material, the carbonyl group provided HTM with a strong defect passivation ability, and the alkylation on the N atom increased the solubility of the molecule, which was believed to provide excellent photovoltaic performance. Besides, MPA-BTTI realized a smoother and more homogeneous surface with a root-mean-square roughness (R_q) of 0.44 nm compared to MPA-BTI with a R_q of 0.96 nm. Thereby, there were better contact interfaces on HTL/perovskite and HTL/electrodes. The glass transition temperature (T_g) values of MPA-BTI and MPA-BTTI were 86 and 256 °C, respectively, which provided highly enhanced device stability of MPA-BTTI-based devices. MPA-BTI exhibited typical J-aggregation in solid state, while MPA-BTTI adopted H-aggregation due to the extended π-system. Consequently, MPA-BTTI realized more effective charge transport and higher hole mobility, compared with MPA-BTI. Moreover, the devices with MPA-BTTI achieved a champion PCE of 21.17%.

In some cases, sulfur atoms were introduced to replace the conventionally used oxygen atoms, because sulfur atoms could passivate the defects of perovskite more effectively by coordinating Pb^{2+} vacancies. Jiang et al. [86] fabricated a new SM-HTM called TPE-S based on tetraphenylethylene (TPE). When used as a dopant-free HTM in the inverted all-inorganic $CsPbI_2Br$ PSCs, the chlorobenzene solution containing TPE-S could be directly processed on the ITO substrate at room temperature without any post-treatment. The optimized all-inorganic device achieved the best PCE value of 15.4% and has a significantly stabilized power output of ∼ 14.3% within 650 s. To demonstrate the versatility of this HTM, this work also produced a hybrid inverted PSC with a TPE-S layer, which achieved a remarkable PCE of 21.0%, close to the record of inverted PSCs (21.6%). Furthermore, Zheng et al. [87] fabricated a new HTM named TXTX-OMeDPA by combining thioxanthenothioxanthene (TXTX) and bis(4-

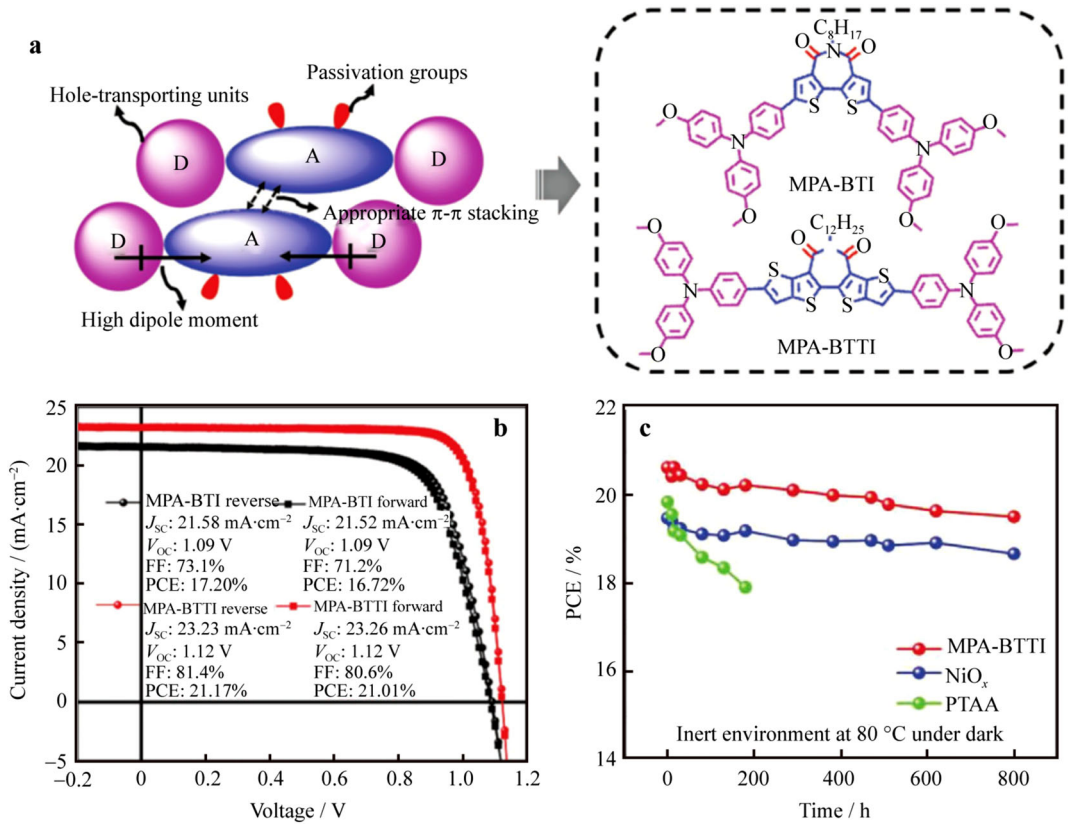

Fig. 10 **a** Schematic diagram of molecular design principles and corresponding chemical structures; **b** *J–V* characteristics; **c** PCE evolution at 80 °C in dark. Reproduced with permission from Ref. [81]. Copyright 2019 John Wiley and Sons

methoxyphenyl)amine. TXTX-OMeDPA film was inferred to have a lateral correlation length of 280 nm, which was larger than that of 105 nm for Spiro-OMeTAD. Besides, the average hole mobility of the TXTX-OMeDPA film was 9.5×10^{-4} $cm^2 \cdot V^{-1} \cdot s^{-1}$, which was more than five times higher than 1.8×10^{-4} $cm^2 \cdot V^{-1} \cdot s^{-1}$ of Spiro-OMeTAD. TXTX-OMeDPA-based PSCs had the characteristics of reduced transportation resistance and expanded interfacial composite resistance, and achieved a notable efficiency of over 22% under AM 1.5 G conditions. The morphological durability of the TXTX-OMeDPA-based film optimized the PSCs with high stability in the aging conditions of both under dark storage at 60 °C and operation under light-soaking at 60 °C.

Pham et al. [82] introduced the cheap anthanthrone dye as a precursor and 1,2-dihydroacenaphthylene (ACE) functional group as the end group for the first time to obtain two HTMs (ACE-ANT-ACE and TPA-ANT-TPA). Under standard illumination (AM 1.5 G and 100 $mW \cdot cm^{-2}$), the average PCEs of devices using ACE-ANT-ACE and TPA-ANT-TPA as HTMs reached 11.4% and 16%, respectively. Interestingly, these PCEs of devices based on TPA-ANT-TPA without any dopant under similar operating conditions were comparable to doped Spiro-OMeTAD devices. In addition, after 20 h in the surrounding environment (room temperature, 58% humidity), the PCE of the unsealed Spiro-OMeTAD-based device retained 2% of its initial value, while the PCE of TPA-ANT-TPA still retained 80% of its initial value. In addition, this team further replaced the core with an electron-deficient biphenyl-fumaronitrile (BPFN) unit to synthesize a novel HTM 2,3-bis(4′-(bis(4-methoxyphenyl)amino)-[1,1′-biphenyl]-4-yl)fumaronitrile (TPA-BPFN-TPA) [83]. Interestingly, the low light performance of undoped TPA-BPFN-TPA-based solar cells also showed significantly improved PCEs of 30.01% and 20.1% over doped Spiro-OMeTAD PSCs' 22.7% and 10% at 1000 lx and 200 lx illumination, respectively.

Besides, Yin et al. [84] successfully designed and synthesized a small-molecule DTP-C6Th based on a simple dithia[3,2-b:2′,3′-d]pyrrole core as an HTM. DTP-C6Th exhibited an appropriate energy level, high hole mobility and high hole extraction efficiency to achieve an efficient and stable PSC. By adding an ultra-thin polymethyl methacrylate passivation layer and appropriately adjusting the composition of the perovskite absorption layer, the optimized PCE of the dopant-free HTM was 21.04%, and the devices showed significantly improved long-term stability. More importantly, the calculation cost of DTP-C6Th

laboratory synthesis was estimated to be ~ 30 $\$\cdot g^{-1}$, which is only one-third of Spiro-OMeTAD. In order to obtain the HTM as cheap and efficient as possible, Cao et al. [85] reported a novel HTM N^2,N^2,N^7,N^7-tetra-p-tolylspiro[fluorene-9,20-[1,3dioxolane]-2,7-diamine (DFH) at a cost of ~ 3 $\$\cdot g^{-1}$ (Fig. 11). The PCE of the PSC devices could be doubled by annealing the amorphous DFH film to a temperature between T_g and temperature of cold crystallization (T_{cc}) to promote dimerization and a small amount of crystallization. The best performance device was obtained by annealing of DFH film at 135 °C. The annealed DFH film quenched >95% of the baseline photoluminescence of the perovskite, indicating that the band arrangement permitted efficient extraction of holes from the perovskite layer. The time resolution of perovskite photoluminescence showed that the annealed DFH extracted 99% of the holes within 20 ns. With annealing at 135 °C, devices containing DFH displayed a very high FF value and achieved an excellent PCE of 20.6%. which were the highest efficiency for dopant-free fluorene-derived HTMs. These simple and inexpensive dopant-free HTMs make high-performance commercial PSCs possible in the future.

9,10-dihydrophenanthrene (DHP) was a rigid conjugated unit, and its two phenyl rings were arranged in an approximately planar conformation. This skeleton was similar to fluorene and just like the methylene group of fluorenyl, the two sp^3-hybridized carbon atoms in DHP could be used as potential sites for further modification to improve thermal stability and solubility and to fine-tune energy levels. For the first time, Dong et al. [88] introduced DHP to fabricate a new type of small-molecule HTM named K-DHP-1 in the photovoltaic field. In this work, bis(4-methoxyphenyl)amine was chosen as the end-capping substituent to achieve an energy level equivalent to H-Spiro-OMeTAD and Spiro-OMeTAD, and a bridged ketal motif was used as the connection. K-DHP-1 was ready to synthesize, was low in cost (~ 11.88 $\$\cdot g^{-1}$) and had good thermal stability. Besides, PSCs prepared based on doped K-DHP-1 achieved an impressive PCE of 20.52%

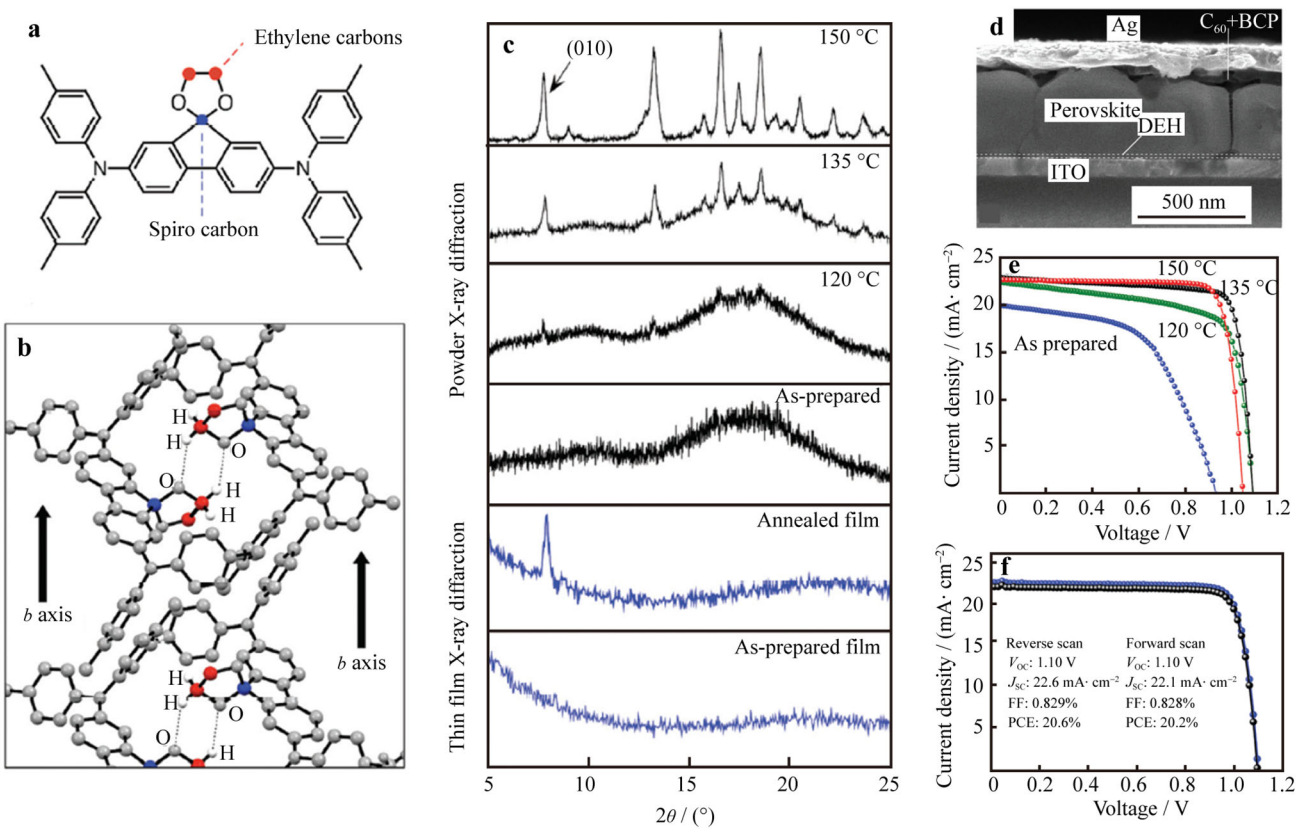

Fig. 11 **a** Molecular structure of DFH with ethylene and Spiro carbon atoms of cyclic 1,3-dioxolane group highlighted in red and blue, respectively; **b** propensity of CH…O interactions between DFH molecules illustrated by a ball-and-stick model derived from X-ray crystallographic data, Spiro carbon and carbon atoms on ethylene group highlighted in blue and red, respectively; **c** powder XRD patterns of DFH before and after thermal crystallization (black) and GIXD traces of 150 nm spin-coated DFH thin films before and after annealing at 150 °C (blue). **d** Cross-sectional SEM image of an inverted (p–i–n) PSC with DFH as HTM; **e** *J*–*V* curves of PSCs with DFH annealed at different temperatures; **f** current–voltage traces of champion device in forward and reverse directions. Reproduced with permission from Ref. [85]. Copyright 2019 Royal Society of Chemistry

and a photovoltage of 1.09 V. Therefore, this work revealed the huge potential of DHP building blocks to further develop low-cost and high-efficiency HTM for PSCs.

4 Research progress of cathode interface materials

With the rapid development of PSCs, scientists have gradually realized that not only the perovskite layer and the HTL were important factors that affect the performance of the device, but it was also crucial to choose the appropriate ETL. For effective PSCs, the ETL should have good energy level matching to achieve effective charge transfer and hole blocking, high electron mobility to ensure fast electron transport, and high stability and low cost.

For PSCs with p–i–n structure, the ETMs were mainly organic materials, such as graphene, fullerene, BCP and their derivatives. The advantage of organic ETMs was that they could be easily processed in solution at low temperature, but their poor environmental stability and poor light stability limited their commercial development. For n–i–p-type PSCs, metal oxides were the most common choice for their ETM. PSC device using mesoporous TiO_2 as the ETM was fabricated in 2009 for the first time. So far, TiO_2 was still the first choice as ETM for PSCs. However, scientists have gradually realized some shortcomings of TiO_2, such as insufficient electron mobility, and the surface adsorption of oxygen and ultraviolet light. These shortcomings were likely to affect the long-term stability of PSC devices and limit the further improvement of device efficiency. At the same time, there were some other metal oxides often used as ETM, such as ZnO [90] and SnO_2 [91]. Besides, scientists developed a method to synthesize perovskite films containing monolithic-like grains with microsize through in situ deposition of octadecylamine-functionalized single-walled carbon nanotubes onto the surface of the perovskite layer, which could enhance the stability of the devices [92]. Herein, we will discuss the recent research progress of metal oxides and organic materials as ETMs for PSCs.

4.1 Inorganic electron transport materials

Because of its suitable conduction band (CB) energy level, wider bandgap, longer electron lifetime and lower manufacturing cost, TiO_2 was usually employed as the ETL for planar PSCs. Generally, in order to obtain a high-performance PSCs, anatase-phase or rutile-phase TiO_2 film was preferred, but high-quality TiO_2 film needed to be sintered above 450 °C [93]. However, high-temperature sintering often made the device manufacturing process more complicated and the cost more expensive, thus limiting its wide application. Therefore, acquiring efficient PSCs through processing TiO_2 at low temperatures became very attractive. There were now atomic layer deposition (ALD) [94], DC magnetron sputtering [95] and chemical bath deposition (CBD) methods [96] that enable the preparation of TiO_2 at low temperatures. However, ALD and DC magnetron sputtering were expensive and difficult to evolve. Moreover, there were many trap states in the TiO_2 films deposited by CBD, and the relatively high density of the electron trap states below the CB of TiO_2 had a great influence on charge transport by producing excessive charge accumulation at the interface of TiO_2 and perovskite [97, 98], which in turn influenced the efficiency and stability of PSCs [99]. Therefore, nanocrystalline TiO_2 treated at low temperature was introduced via a CBD method at 70 °C and an excellent PCE was obtained [100]. In addition, graphene nanocomposites and TiO_2 nanoparticles were used for ETLs treated at low temperature in PSCs, and a remarkable PCE of 15.6% has been achieved [101]. Recently, Zhou et al. [102] introduced photoactivated transition metal dihalide quantum dots (TMDCs QDs, MoS_2 and $MoSe_2$) to enhance low-temperature processed TiO_2 ETL for all-inorganic $CsPbBr_3$ PSCs without HTL and precious metal electrode. Different kinds of low-temperature processed ETLs such as TiO_2 [103], ZnO [90], WO_x [96], SnO_2 [92] and fullerene derivatives [104] were already reported.

4.1.1 Modification via doping

Doping of TiO_2 was one of the most effective methods to reduce inappropriate charge accumulation in PSCs, ensure effective interface electron injection and improve the CB level of the TiO_2 layer. Appropriate substitution of Y^{3+}, Al^{3+}, Sn^{4+}, Nb^{5+} and Mg^{2+} has been introduced to improved properties of TiO_2 for PSCs. Sn^{4+} was successfully incorporated into the TiO_2 lattice without forming a second phase.

Compared with the original TiO_2, Sn-doped TiO_2 was more efficient in the extraction and transport of photogenerated electrons, showing a lower density of trap states and higher electrical conductivity. Owing to the increase in carrier transfer speed and charge collection efficiency, a higher J_{SC} was successfully obtained, resulting in a higher fill factor (FF) and better PCE [105]. Furthermore, the demonstration of morphology and topographic images was studied by observing the surface morphology of various Sn/TiO_2 layers through multi-functional FE-SEM and AFM. It was discovered that TiO_2 with the Sn doping would slightly change the RMS roughness. When the doping level up to 1.0 mol%, the surface morphology became smoother and it might be more suitable for manufacturing efficient PSCs

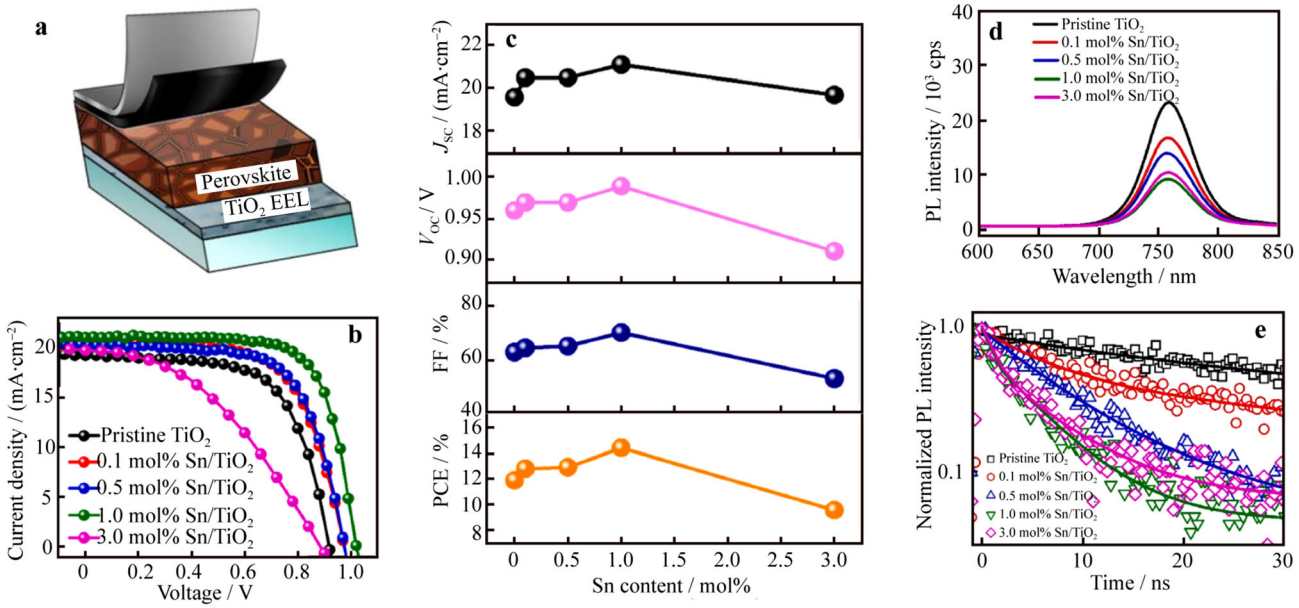

Fig. 12 **a** Schematic diagram of devices; **b** *J–V* characteristics of PSCs based on various Sn/TiO_2 EEL; **c** correlation between photovoltaic characteristics (V_{OC}, J_{SC}, FF and PCE) and Sn doping concentration; **d** PL spectra and **e** transient TRPL plots of device with structure of $CH_3NH_3PbI_{3-x}Cl_x$/(Sn/TiO_2)/FTO. Reproduced with permission from Ref. [106]. Copyright 2020 Elsevier

(Fig. 12) [106]. Large-scale TiO_2 and Nb-doped TiO_2 could be deposited as ETL for PSCs by low-temperature CBD method. Nb-doped TiO_2 exhibited better conductivity and mobility and reduced the density of trap states, resulting in reduced electron recombination, enhanced electron transport and increased PSC stability. PSCs with Nb-doped TiO_2 showed great stability, maintaining 90% of its initial value in the air over 1200 h and had better thermal stability than PSC with pure TiO_2 [107]. In addition, a new method steam-annealing (SA) was introduced into the TiO_2 ETL doping process, and a highly crystalline Nb-TiO_2 thin film was successfully prepared. By changing the concentration of Nb doping, their CB level reduced lower. At the same time, due to the high J_{SC} value of about 25 mA·cm^{-2}, the PCEs of devices achieved the highest value of 21.3% without a loss of V_{OC} [108].

Al-doped TiO_2 effectively reduced the trap position inside the crystal, which led to a wider bandgap. Secondly, the Al-doped TiO_2 layer exhibited a smooth surface morphology, which affected the formation of a highly crystalline upper photosensitive layer and reduced the interface recombination between the active layer and the electron extraction layer [109]. The decrease in the trap-filling limit voltage (V_{TFL}) of the TiO_2 dense layer indicated that the trap density of the Ru:TiO_2 film was lower than that of the original TiO_2 film. PSCs based on 1 mol% Ru:TiO_2 exhibited a suitable band gap, low resistivity and high carrier density. Compared with the undoped TiO_2, doping with Ru enhanced the transfer of charge of the dense layer/mesoporous layer interface, thereby reducing the hysteresis of the devices. The PCE of the Ru-doped compact TiO_2 film-based PSCs increased from 13.42% to 15.7% [110]. Attractively, Ni-doped TiO_2 improved the conductivity and carrier mobility, as well as the positive shift of the Fermi level, and achieved the best PCEs of carbon-based PSCs from 15.82% to 17.46% [111]. As for other metal oxides ETL, Halvani et al. [112] fabricated a series of SnO_2 ESL via low-temperature, solution-processed CBD method without using spin coating. When the amount of Nb was optimally doped (5%), the PCEs of devices deposited only by CBD were increased from 19.0% to 20.1%. More importantly, under Nb-doped, the FF of the devices significantly increased, mostly observed in the series resistance, and this result was reproducible. Here, we show a summary of the device performance of ETLs with different substitutions in Table 2 [105–112].

4.1.2 Modification via changing of chemical structure

It is well known that there were many types of TiO_2 crystals. Studies have shown that rutile TiO_2 had higher electrical conductivity, faster electron transport, better interface contact with the perovskite layer and lower defect density. These factors promoted the extraction and collection of charges and reduce carrier recombination. As a result, a 20.9% champion PCE and a large V_{OC} of 1.17 V were obtained on devices with RT-ETL, which was significantly higher than devices with anatase TiO_2 [113]. Besides, $TiCl_4$ treatment for compact TiO_2 was used to enhance the photovoltaic performance of PSCs. TiO_2 layer with an appropriate $TiCl_4$ treatment provided a smooth

Table 2 Summary of device performances of ETL doping with different additives

ETLs modified with substitution	V_{OC}/V	J_{SC}/(mA·cm^{-2})	FF/%	PCE/%	Refs.
Sn–TiO_2	1.10	21.53	72.7	17.20	[105]
Sn–TiO_2	1.01	21.90	73.1	15.20	[106]
Nb–TiO_2	1.10	22.86	76.5	19.23	[107]
Nb–TiO_2	1.11	23.50	76.0	20.00	[108]
Al–TiO_2	0.96	19.23	69.0	12.52	[109]
Ru–TiO_2	0.99	21.91	72.1	15.70	[110]
Ni–TiO_2	1.07	22.41	72.6	17.46	[111]
Nb–SnO_2	1.16	22.77	74.7	20.47	[112]

surface fully covering the conductive electrode and improved the interface contact between the electron extraction layer and the active layer [114]. In order to further explore the effect of $TiCl_4$ treatment on the TiO_2 layer, Shahvaranfard et al. [115] modified the TiO_2 rutile nanorods by $TiCl_4$ treatment combined with $PC_{61}BM$ single-layer deposition. The $TiCl_4$ and $PC_{61}BM$ treatments were expected to affect the charge extraction on the entire TiO_2 ETL/perovskite interface. Through several sets of control experiments, this work confirmed the benefits of using nanorod (NR) arrays as nanostructured ETLs and confirmed the synergistic effects produced by surface modification of TiO_2 NPs. The dual modification of TiO_2 NR ETL was combined with $TiCl_4$ treatment and subsequent deposition of $PC_{61}BM$. After double modification, the greatest improvement in equipment performance was observed. This improvement showed a significant dependence on the concentration of $TiCl_4$, especially when the TiO_2 NRs were treated with 100×10^{-3} mol·L^{-1} $TiCl_4$ solution. Under optimized conditions, these devices could provide excellent photovoltaic parameters, with V_{OC} up to 1.09 V, J_{SC} improvement of 22.8 mA·cm^{-2}, FF improvement of 74% and average PCE of 17.9% (Fig. 13).

Besides, DA was introduced to modify the TiO_2 layer to passivate its surface. After DA capping treatment, the oxygen vacancies in TiO_2 nanoparticles were effectively passivated and the deep trap states on the surface were alleviated [116]. At the same time, due to the strong adhesion function of DA itself, the interface between TiO_2 and the perovskite film was improved by greatly suppressing the charge recombination loss. The introduction of DA had strong electron donor ability and interface cross-linking, which was conducive to charge transfer and transfer charge accumulation between the TiO_2/perovskite interface. Most importantly, the amino group in DA could passivate uncoordinated Pb atoms and reduced the Pb–I/Br anti-site defects on the perovskite interface. It could effectively fill in the trap status. As expected, DA-encapsulated TiO_2 ETL could effectively improve the PCE of PSCs. Compared with the control device, devices dealing with DA achieved the highest PCE of 20.93%, and the hysteresis was negligible. In addition, the UV stability of the unencapsulated devices was significantly improved compared to the control device with pure TiO_2. After 400 h of irradiation, the PCE of the devices based on pure TiO_2 dropped to almost zero. On the contrary, after 1200 h of continuous full daylight without any UV filter, the device based on DA-terminated TiO_2 retained almost 80% of its initial performance (Fig. 14).

SnO_2 was a promising substitute for TiO_2 as the ETM. But devices with SnO_2 still existed the hysteresis problem. To solve the hysteresis and improve the performance of devices, Liu et al. [117] employed the common and cheap inorganic compound ammonium chloride (NH_4Cl) to assimilate into commercial SnO_2 hydrocolloid dispersions and found that NH_4Cl induced coagulation of SnO_2

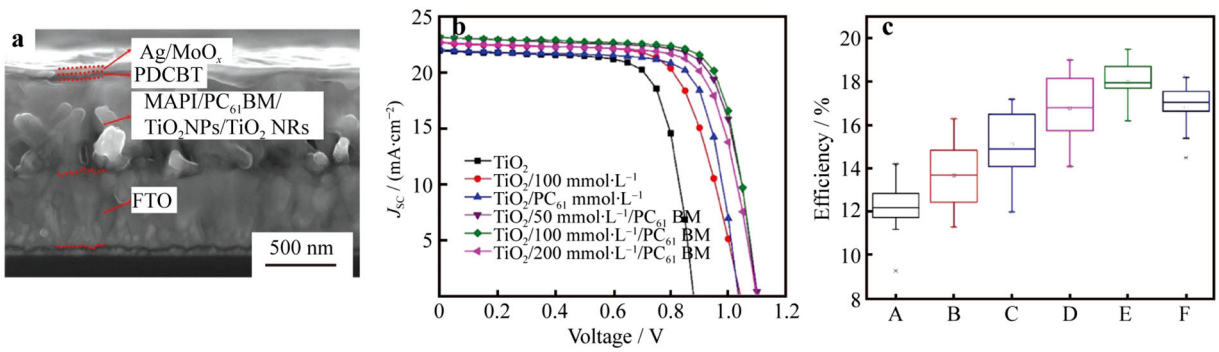

Fig. 13 **a** Cross-sectional SEM image of devices with TiO_2 modified by different methods; **b** current density–voltage characteristics of champion devices with different modifications for ETL; **c** PCE for devices constructed from A: pristine NRs, B: NRs treated with 100×10^{-3} m $TiCl_4$, C: NR coated with $PC_{61}BM$, D: NR/50×10^{-3} m $TiCl_4$/$PC_{61}BM$, E: NR/100×10^{-3} m $TiCl_4$/$PC_{61}BM$ and F: NR/200×10^{-3} m $TiCl_4$/$PC_{61}BM$. Reproduced with permission from Ref. [115]. Copyright 2020 John Wiley and Sons

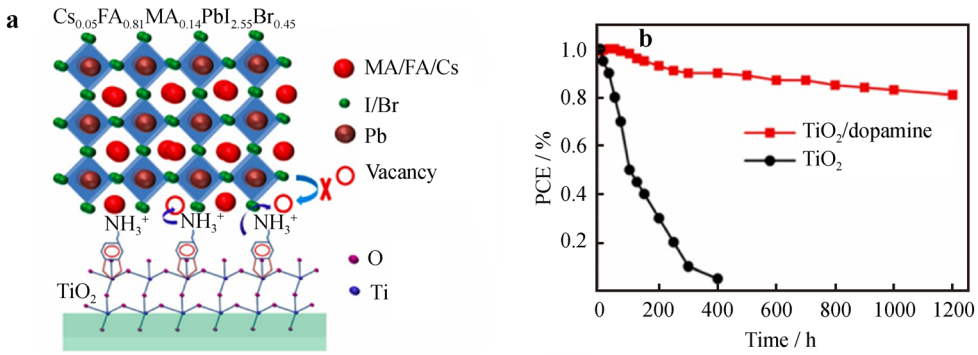

Fig. 14 **a** Schematic of DA function on TiO_2/perovskite layer interface; **b** normalized PCE change of devices with TiO_2 and DA-capped TiO_2 as ETLs under continuous full-sun illumination in nitrogen atmosphere. Reproduced with permission from Ref. [116], Copyright 2019 Elsevier

colloids, increased electron mobility and acquired a suitable CB energy level to adapt to perovskite layer. In addition, the introduction of NH^{4+} and Cl^- at the ETL/perovskite interface could optimize the ETL/perovskite interface by suppressing the formation of deep defects. Due to improved charge transport and reduced charge recombination, devices based on NH_4Cl-modified SnO_2 could achieve an excellent PCE of 21.38%, which was better than the PCE (18.71%) of devices based on original SnO_2. At the same time, the hysteresis was negligible and the stability of devices was greatly improved. Furthermore, Chen et al. [118] introduced a new type of multifunctional 4-methylimidazole acetic acid hydrochloride (ImAcHCl) chemical connector into SnO_2 ETL. This linking agent could form a chemical bridge between SnO_2 and perovskite with ester bonds. And the imidazolium cation in ImAcHCl interacts electrostatically with the iodide anion in the perovskite. After ImAcHCl modification, the conductivity of the SnO_2 film was improved, which might help promote the interface electron transfer. Additionally, the ImAcHCl layer at the SnO_2/perovskite interface could effectively passivate the parasitic defects generated by imidazolium cations or Cl^- in the perovskite, thereby inhibiting the non-radiative recombination of the interface and finally improving the V_{OC}. By using multifunctional ImAcHCl chemical linker in between SnO_2 and perovskite, a PCE of 21% was achieved with long-term stability maintaining 94% of initial PCE after 35 days.

4.2 Organic electron transport materials

In order to obtain excellent performance ETMs for PSCs, various groups have designed organic molecule-based materials through appropriate molecular design. All molecular structures of organic ETMs for PSCs are shown in Fig. 15.

The perovskite/ETM interface played a significant role in the planar PSCs, which was related to the electron extraction process, hysteresis and device stability. Fullerene could passivate the trap states on the surface and grain boundaries of the perovskite film. It significantly suppressed the current–voltage hysteresis and increased the PCE of PSCs [119]. In order to adjust the Fermi level of C_{60} and increase the conductivity, Ueno et al. [120] introduced a method of doping C_{60} with Li^+ without causing crystal distortion. C_{60} and Li@C_{60} were mixed and then spin-coated on an ITO substrate to prepare a C_{60}:Li@C_{60} hybrid film. Under a suitable doping concentration condition, the PCE of the PSC devices became optimal. Wang et al. [121] employed polar carboxyl-terminated fulleropyrrolidine (C_{60} pyrrolidine tris-acid, CPTA) and PbI_2 to successfully fabricate a new ETL CPTA:PbI_2. PSC devices based on CPTA:PbI_2 ETL have reduced non-radiative defect density and had a superior FF of more than 80%. Besides, in order to improve the effect of oxygen vacancies and structural defects in the TiO_2 layer on the recombination loss, Ranjan et al. [122] added a layer of $PC_{60}BM$ as a buffer layer between the perovskite layer and c-TiO_2. After the device was adjusted, the quality of the interface between the constituent layers was improved. Thereby, the PCE of devices increased by about 40% after 50 h. Additionally, before 150 h, the charge transfer in the devices was great. After 50 h, due to the degradation of the perovskite layer at the perovskite/$PC_{60}BM$ interface, the main reason for the degradation of the device performance was the recombination of charges. Furthermore, Li et al. [123] proposed to employ ultra-thin [6,6]-phenyl-C_{61}-butyric acid methylester ($PC_{61}BM$) as a buffer layer between the perovskite layer and the C_{60} layer to improve the interface. The pinholes of the rough surface perovskite film were repaired and smoothed by the ultra-thin $PC_{61}BM$, and the surface traps were also eliminated. Finally, the PCE of PSCs reached 20.07%, and the PSCs processed by ultra-thin $PC_{61}BM$ had better stability.

Bathocuproine (BCP) buffer layer was commonly used for PSCs to achieve high performance. Chen et al. [124]

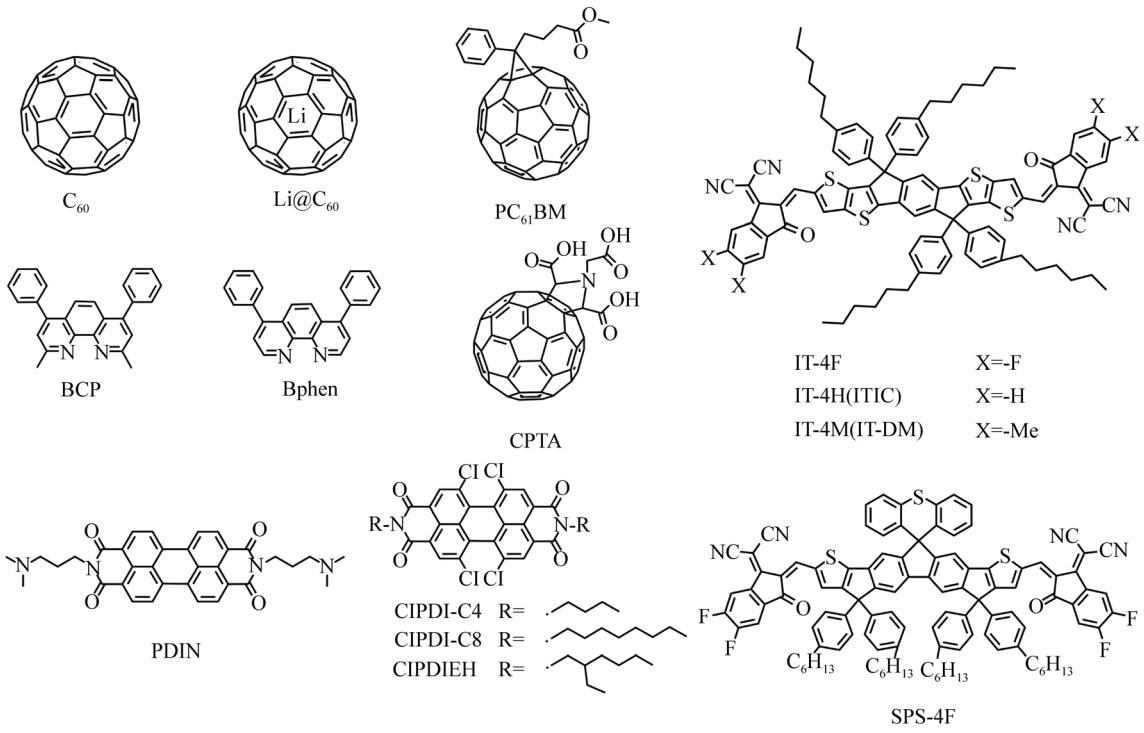

Fig. 15 Molecular structures of organic electron transport materials

adjusted the thickness of the BCP film, and the PSC devices prepared with an optimal thickness of 5 nm successfully achieved a high PCE of 17.9%. Furthermore, Yang et al. [125] developed a PSC device with high PCE and good photostability with bathophenanthroline (Bphen, 4,7-diphenyl-1,10-phenanthroline) as ETL. The embedding of the Bphen layer effectively promoted the shunt resistances (R_{sh}), leading to the increase of V_{OC}, FF and PCE, and promoted the charge transfer. Most importantly, the Bphen layer greatly promoted the stability of the device by avoiding the catalytic effect of TiO_2 on the decomposition of the perovskite film.

Liu et al. [126] developed a series of semiconductors based on ITIC-like small molecules IT-4X, whose difference was the introduction of different substituents. When the substituent was methyl, the novel semiconductor was called IT-4 M. More importantly, a champion PCE of 17.65% was achieved by devices based on IT-4 M as ETL, which was higher than that of the devices with PCBM under the same conditions. In addition, due to the superior hydrophobicity, all PSCs with IT-4X ETL showed higher long-term stability under environmental conditions than the reference devices (Fig. 16a–c). Hu et al. [127] fabricated a novel Spiro ring-based ETM called SFS-4F. The S atoms in the parent Spiro ring could interact with the Pb in the perovskite layer and led to effective surface trap passivation. The rigid coplanar structure of the molecule could prevent rotation disorder and reduced recombination energy, thereby enhancing carrier mobility. More importantly, the PSC devices with SPS-4F as ETM showed a remarkable PCE of up to 20.31% and a high V_{OC} of about 1.15 eV (Fig. 16d–f).

In recent years, n-type organic semiconductors based on polyene diimide (PDI) derivatives have unique advantages such as low mass production costs, strong synthesis versatility, tunable energy levels, good electrochemical stability and light stability. Miao et al. [128] used perylene diimides derivative (PDIN) to easily form a high-quality PDIN film on the perovskite layer while avoiding the corrosion problem of alcohol solution. The PCE of the devices with PDIN as the ETL reached 15.28%, which was much higher than that of the devices with only $PC_{61}BM$. Furthermore, Jiang et al. [129] used TPE-PDI4 as ETL to develop a PSC device with a high PCE of 18.78%. TPE-PDI4 had better water resistance than PCBM and could more effectively protect the underlying perovskite layer. Therefore, devices with ETL based on TPE-PDI4 exhibited enhanced stability. Besides, Singh et al. [130] developed the core-twisted ClPDI dye as ETM for high-performance PSCs. The influence of alkyl substitutions of different sizes on the molecular arrangement related to photovoltaic performance was systematically studied. ClPDI-C4 with the shortest alkyl side chain had electron mobility as high as 1.3×10^{-3} $cm^2 \cdot V^{-1} \cdot s^{-1}$ and a higher R_{rec} that inhibited

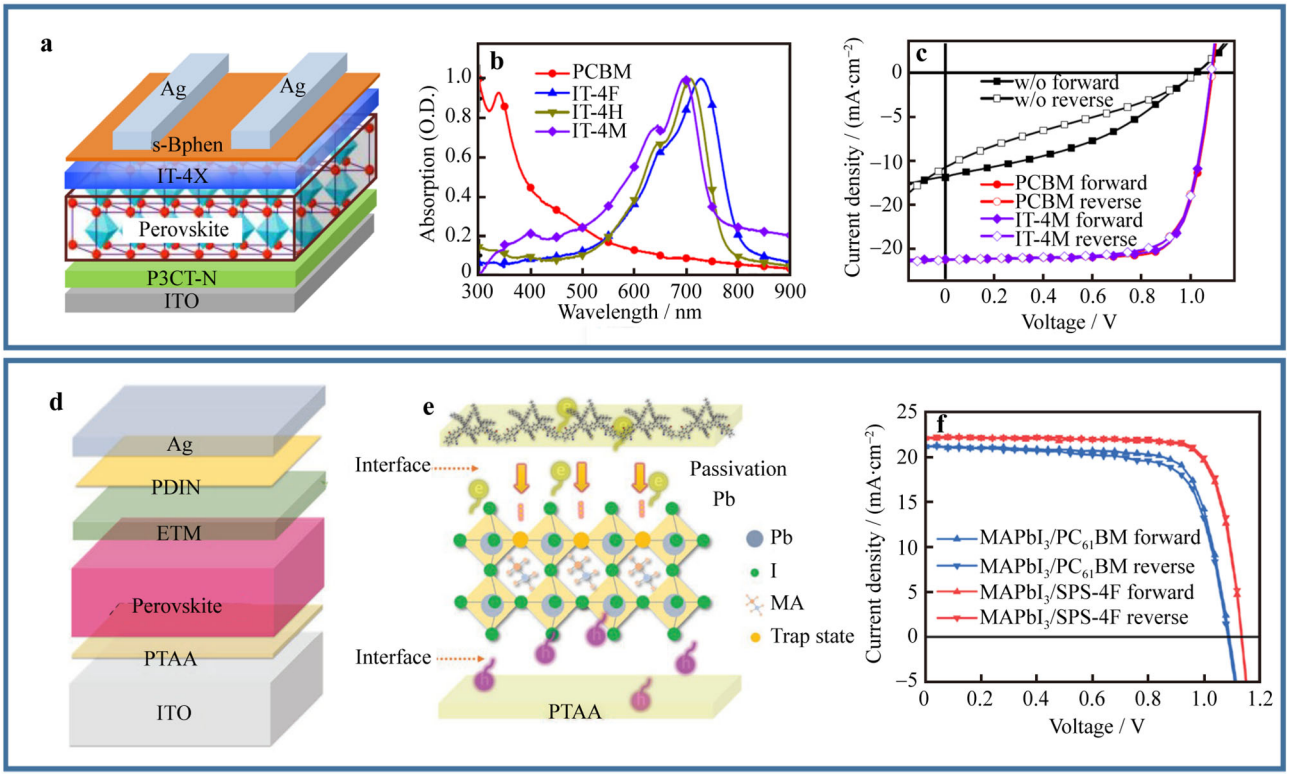

Fig. 16 **a** Schematic of inverted PSCs with IT-4X; **b** absorption spectra of PCBM, IT-4F, IT-4H and IT-4 M films; **c** *J–V* curves measured under forward- and reverse-scan directions. Reproduced with permission from Ref. [126]. Copyright 2019 Royal Society of Chemistry. **d** Schematic of inverted PSC devices with SPS-4F; **e** schematic for passivation effect of SPS-4F on top surface of perovskite layer; **f** current density–voltage (*J–V*) curves of devices with SPS-4F and $PC_{61}BM$ as ETL. Reproduced with permission from Ref. [127]. Copyright 2019 John Wiley and Sons

the photogenerated charge recombination at the perovskite/ClPDI-C4 interface, which was beneficial to improve J_{SC} and FF. Therefore, an excellent champion PCE of 17.3% was achieved by the device based on ClPDI-C4.

Recently, poly[(9,9-dioctyl-2,7-fluorene)-alt-(9,9-bis(3′-(N,N-dimethylamino)propyl)-2,7-fluorene)] (PFN) has been used as a cathode interface material in perovskite solar cell devices. There were two different types of side chains in PFN molecules: hydrophobic alkyl groups and hydrophilic amine groups. PFN could be used as a cathode modification layer because it could form a dipole at the interface of ITO, to reduce the work function of ITO, adjust the energy level between ITO and the acceptor material and promote the transport of carriers.

In recent years, Huang's group has made tremendous efforts in the application and inherent mechanism of PFN and its derivative [131–133]. Wang et al. [134] employed changes in interfacial dipole and interfacial contact angle during self-assembly to investigate a spontaneous interfacial dipole orientation effect in acetic acid dissolved PFN. Moreover, PFN was used to modify the surface properties of Zn_2SnO_4 thin-film (ZSO/PFN) i-PSCs with the ZSO/PFN EEL, which exhibited a PCE of 8.44% owing to improved interfacial contact with the active layer and the better energy level alignment between the active layer and electrode. As the amount of PFN doped into the active layer increased, the PCEs of the devices decreased due to the increased leakage current, the reduced aggregation of P3HT and the decreasing phase separation. In the PTB7:PCBM bulk heterojunction (BHJ) mixture [133], successful doping of multifunctional conjugated polymer PFN with terminal amino electron-donating groups would achieve vertical self-assembly of conjugated PFN molecules after drying. Encouragingly, device performance was achieved in the one-step coating PFN:BHJ PSC with ITO as the cathode, which was comparable to that of the two-step coating PSC.

A solution-processed amino-functionalized copolymer semiconductor (PFN-2TNDI), in conjunction with a planar n–i–p heterojunction, exhibited an amazing PCE of similar to 16% under standard illumination test conditions [135]. Besides, in the p–i–n planar heterojunction organometal PSCs, PFN-2TDI as ETL enhanced efficiency from 12.9% to 16.7% compared to PCBM [136]. In this work, the passivation effect produced by the dative–covalent combination of the Pb atom and the rich-electron nitrogen atom

was proposed for the significant enhancement of PSC performance [137].

Benzobisthiadiazole (BBT) is an important component of organic conductors, donor–acceptor low-gap polymers and near-infrared dyes because of its strong electron-withdrawing properties. Zhu et al. [138] designed and synthesized a benzobis(thiadiazole)-based small molecule called B2F and applied such a structure as an efficient electron extraction material in inverted PSCs (Fig. 17). The device based on a single B2F layer exhibited a PCE of 12.35%. Further improvement of PCE could be achieved by using B2F as an interlayer for the perovskite and C_{60}/BCP as ETL and hole-blocking layers to enhance the electron extraction and prevent carrier leakage. A champion PCE of 17.18% was obtained with a V_{OC} of 1.052 V, a J_{SC} of 20.63 mA·cm^{-2}, and an FF of 79.15%. The good performance could be attributed to the suitable energy level of B2F with the perovskite layer. Furthermore, novel small molecules B2T (Fig. 17) based on benzobis(thiadiazole) were designed and compared with B2F as ETMs for PSCs [139]. Both B2T and B2F exhibited an efficient electron transporting ability because of the high electron affinity of benzobis(thiadiazole) unit. Devices with B2T and B2F as ETMs exhibited a PCE over 13% with good reproducibility and negligible photocurrent hysteresis.

5 Summary and outlook

In summary, the recent development of interface materials for PSCs is comprehensively reviewed and summarized. The continuous efforts are still required in order to obtain high PCE and stability of PSC devices for large-scale applications of commercialization. We would like to summarize the latest research progress of anode and cathode interface materials and provide some outlooks as following.

For the anode interface, PEDOT:PSS is by far the most successful conducting polymer which is commercially available. This review discusses the conductive mechanism of PEDOT:PSS and its modification with a novel dispersant to achieve excellent device performance. The development trend of conductive polymer materials should be mainly in the following aspects: (a) improving its own conductivity and stability; (b) enhancing the mechanical properties and processing capability of the composite material through chemical doping; and (c) preparing novel types of conductive polymer materials. Besides, in this review, we mainly emphasized undoped SM-HTMs, which have excellent solution processing properties and high PCE. Most high-efficiency SM-HTMs recently reported have a planar rigid core and contain donor units, which make them have excellent hole transport and film-forming capabilities. We could propose the design principles of undoped SM-HTM as follows: (a) the core with strong interaction force which will promote the intermolecular interaction between HTM and perovskite for defect passivation; (b) proper solubility and solution processability; (c) aligning the HOMO/LUMO energy level to effectively extract light holes and block photogenerated electrons; and (d) excellent thermal/chemical stability.

For the cathode interface materials, we discuss work dedicated to optimizing ETL and modifying the interface on the ETL/perovskite layer and the interface on the ETL/metal electrode. Various ETMs have been developed and applied in PSCs, including some metal oxides, such as TiO_2, SnO_2, and some organic compounds, such as C_{60}, $PC_{61}BM$, PDI, ITIC, PFN, BBT and their derivatives. The proper work function, good electron transfer capability and low recombination rate at the interface are the important

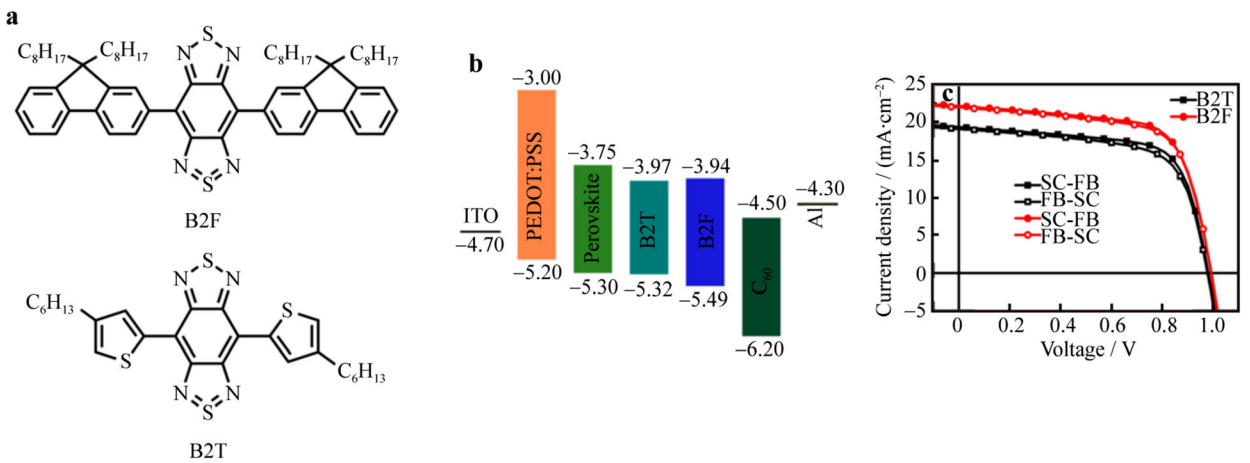

Fig. 17 **a** Chemical structure of B2F and B2T; **b** energy level alignment of materials; and **c** *J–V* characteristic curves of devices with B2T and B2F as ETLs. Reproduced with permission from Ref. [139]. Copyright 2019 Elsevier

issues to be considered. Through different mechanisms, these modifications have improved the performance of PSCs devices and this has become an important topic to develop high-performance PSCs. The excellent ETMs usually show several significant characteristics as followings: (1) excellent solubility in the orthogonal solvent of the perovskite crystal and tendency to form a smooth surface film, (2) suitable LUMO energy compatible with those of the perovskite layers to achieve effective electron extraction, (3) high electron mobility, (4) low cost of synthesis and (5) thermal/electrochemical stability and photostability.

In short words, PSCs are ideal candidates for commercial development due to their tunable bandgaps, high PCE over 25%, large-scale preparation and easy fabrication. Moreover, perovskite-based tandem solar cells have realized a remarkable record PCE of 29.1%, high V_{OC}, good indoor performance and covering wide spectra, which enable them for unique applications in addition to the dominate common applications in photovoltaic devices when combining with the commercial Si modules [140]. Besides, the interface materials are considered to be fundamentally important in further improving PSC performance based on novel modification [141–144], as well as Spiro-based derivatives [145, 146] and other potential interface materials [147, 148]. Therefore, the development of new interface materials and engineering will still be significantly important for the final industrial commercialization of PSCs.

Acknowledgements This work was financially supported by the National Natural Science Foundation of China (No. 51973063), the Pearl River S&T Nova Program of Guangzhou (No. 201710010194) and the Tip-top Scientific and Technical Innovative Youth Talents of Guangdong Special Support Program (No. 2019TQ05C890).

References

[1] Hammarstrom L. Artificial photosynthesis and solar fuels. Accounts Chem Res. 2009;42(12):1859.
[2] Kurtz SR, Allerman A, Jones E, Gee J, Banas J, Hammons BJ. InGaAsN solar cells with, 1.0 eV band gap, lattice matched to GaAs. Appl Phys Lett. 1999;74(5):729.
[3] Mathew S, Yella A, Gao P, Humphry-Baker R, Curchod BF, Ashari-Astani N, Tavernelli I, Rothlisberger U, Nazeeruddin MK, Grätzel M. Dye-sensitized solar cells with 13% efficiency achieved through the molecular engineering of porphyrin sensitizers. Nature Chemistry. 2014;6(3):242.
[4] Liu Q, Jiang Y, Jin K, Qin J, Xu J, Li W, Xiong J, Liu J, Xiao Z, Sun K, Yang S, Zhang X, Ding L. 18% efficiency organic solar cells. Sci Bull. 2020;65(4):272.
[5] Cui Y, Yao H, Zhang J, Xian K, Zhang T, Hong L, Wang Y, Xu Y, Ma K, An C, He C, Wei Z, Gao F, Hou J. Single-junction organic photovoltaic cells with approaching 18% efficiency. Adv Mater. 2020;32(19):1908205.
[6] Kojima A, Teshima K, Shirai Y, Tsutomu M. Organo metal halide perovskites as visible-light sensitizers for photovoltaic cells. J Am Chem Soc. 2009;131(17):6050.
[7] Green MA, Dunlop ED, Levi DH, Hohl-Ebinger J, Yoshita M, Ho-Baillie AWY. Solar cell efficiency tables (version 54). Prog Photovoltaics Res Appl. 2019;27(7):565.
[8] Niu T, Zhu W, Zhang Y, Xue Q, Jiao X, Wang Z, Xie YM, Li P, Chen R, Huang F, Li Y, Hin-Lap Y, Cao Y. D-A-π-A-D type dopant-free hole transport material for low-cost, efficient and stable perovskite solar cells. Joule. 2021;5(1):249.
[9] Yang G, Tao H, Qin P, Ke W, Fang G. Recent progress in electron transport layers for efficient perovskite solar cells. J Mater Chem A. 2016;4(11):3970.
[10] Yao D, Mao X, Wang X, Yang Y, Hoang MT, Du A, Waclawik ER, Wilson GJ, Wang H. The effect of ethylene-amine ligands enhancing performance and stability of perovskite solar cells. J Power Sources. 2020;463:228210.
[11] Ham ND, Yang Y, Hoang MT, Wang T, Tiong VT, Wilson GJ, Wang H. 1D pyrrolidinium lead iodide for efficient and stable perovskite solar cells. Energy Technol. 2020;8(4):1900918.
[12] Yao D, Zhang C, Zhang S, Yang Y, Du A, Waclawik E, Yu X, Wilson GJ, Wang H. 2D-3D mixed organic-inorganic perovskite layers for solar cells with enhanced efficiency and stability induced by n-propylammonium iodide additives. ACS Appl Mater Interfaces. 2019;11(33):29753.
[13] Zhang C, Wang S, Zhang H, Feng Y, Tian W, Yan Y, Bian J, Wang Y, Jin S, Zakeeruddin S, Grätzelb M, Shi Y. Efficient stable graphene-based perovskite solar cells with high flexibility in device assembling via modular architecture design. Energy Environ Sci. 2019;12(12):3585.
[14] Jiang Y, Liu T, Zhou Y. Recent advances of synthesis, properties, film fabrication methods, modifications of poly (3, 4--ethylenedioxythiophene), and applications in solution-processed photovoltaics. Adv Funct Mater. 2020:2006213.
[15] Li Y, Meng H, Liu T, Xiao Y, Tang Z, Pang B, Li Y, Xiang Y, Zhang G, Lu X. 8.78% efficient all-polymer solar cells enabled by polymer acceptors based on a B ← N embedded electron-deficient unit. Adv Mater. 2019;31(44):1904585.
[16] Zamora-Sequeira R, Ardao I, Starbird R, García-González CA. Conductive nanostructured materials based on poly-(3, 4--ethylenedioxythiophene)(PEDOT) and starch/κ-carrageenan for biomedical applications. Carbohydr Polym. 2018;189(9):304.
[17] Wong A, Santos AM, Silva TA, Fatibello-Filho O. Simultaneous determination of isoproterenol, acetaminophen, folic acid, propranolol and caffeine using a sensor platform based on carbon black, graphene oxide, copper nanoparticles and PEDOT: PSS. Talanta. 2018;183(10):329.
[18] Xu G, Jarjes ZA, Desprez V, Kilmartin PA, Travas-Sejdic J. Sensitive, selective, disposable electrochemical dopamine sensor based on PEDOT-modified laser scribed graphene. Biosens Bioelectron. 2018;107(8):184.
[19] Shi H, Liu C, Jiang Q, Xu J. Effective approaches to improve the electrical conductivity of PEDOT: PSS: a review. Adv Electron Mater. 2015;1(4):1500017.
[20] Groenendaal L, Zotti G, Aubert PH, Waybright SM, Reynolds JR. Electrochemistry of poly (3, 4-alkylenedioxythiophene) derivatives. Adv Mater. 2003;15(11):855.
[21] Groenendaal L, Jonas F, Freitag D, Pielartzik H, Reynolds JR. Poly (3, 4-ethylenedioxythiophene) and its derivatives: past, present, and future. Adv Mater. 2000;12(7):481.
[22] Tran-Van F, Garreau S, Louarn G, Froyer G, Chevrot C. Fully undoped and soluble oligo (3, 4-ethylenedioxythiophene) s:

spectroscopic study and electrochemical characterization. J Mater Chem. 2001;11(5):1378.
[23] Jonas F, Heywang G, Schmidtberg W, Heinze J, Dietrich M. Polythiophenes, process for their preparation and their use. U. S. Patent 4,959,430. 1990.
[24] Greczynski G, Johansson N, Lögdlund M, Pettersson L, Salaneck WR, Horsburgh L, Monkman A, dos Santos D, Bredas J. Electronic structure of pristine and sodium doped poly (p-pyridine). J Chem Phys. 2001;114(9):4243.
[25] Chen ZX, Li Y, Huang F. Persistent and stable organic radicals: design, synthesis and applications. Chem. 2021;7(2):288.
[26] Põldsalu I, Harjo M, Tamm T, Uibu M, Peikolainen AL, Kiefer R. Inkjet-printed hybrid conducting polymer-activated carbon aerogel linear actuators driven in an organic electrolyte. Sens Actuators B Chem. 2017;250(8):44.
[27] Cho SR, Porte Y, Kim YC, Myoung JM. Effect of nonionic surfactant additive in PEDOT: PSS on PFO emission layer in organic–inorganic hybrid light-emitting diode. ACS Appl Mater Interfaces. 2018;10(11):9612.
[28] Zhou L, Yu M, Chen X, Nie S, Lai WY, Su W, Cui Z, Huang W. Screen-printed poly (3, 4-ethylenedioxythiophene): poly (styrenesulfonate) grids as ITO-free anodes for flexible organic light-emitting diodes. Adv Funct Mater. 2018;28(11):1705955.
[29] Ji G, Wang Y, Luo Q, Han K, Xie M, Zhang L, Wu N, Lin J, Xiao S, Li YQ. Fully coated semitransparent organic solar cells with a doctor-blade-coated composite anode buffer layer of phosphomolybdic acid and PEDOT: PSS and a spray-coated silver nanowire top electrode. ACS Appl Mater Interfaces. 2018;10(1):943.
[30] Wu Z, Yu Z, Yu H, Huang X, Chen M. Effect of trifluoroacetic acid treatment of PEDOT: PSS layers on the performance and stability of organic solar cells. J Mater Sci Mater Electron. 2018;29(8):6607.
[31] Fan X, Nie W, Tsai H, Wang N, Huang H, Cheng Y, Wen R, Ma L, Yan F, Xia Y. PEDOT: PSS for flexible and stretchable electronics: modifications, strategies, and applications. Adv Sci. 2019;6(19):1900813.
[32] He X, Yang W, Mao X, Xu L, Zhou Y, Chen Y, Zhao Y, Yang Y, Xu J. All-solid state symmetric supercapacitors based on compressible and flexible free-standing 3D carbon nanotubes (CNTs)/poly (3,4-ethylenedioxythiophene)(PEDOT) sponge electrodes. J Power Sources. 2018;376(9):138.
[33] Li X, Deng X, Li Q, Huang S, Xiao K, Liu Z, Tong Y. Hierarchical double-shelled poly (3, 4-ethylenedioxythiophene) and MnO_2 decorated Ni nanotube arrays for durable and enhanced energy storage in supercapacitors. Electrochim Acta. 2018;264(7):46.
[34] Correa-Baena JP, Abate A, Saliba M, Tress W, Jacobsson TJ, Grätzel M, Hagfeldt A. The rapid evolution of highly efficient perovskite solar cells. Energy Environ Sci. 2017;10(3):710.
[35] Kim J, Kim G, Back H, Kong J, Hwang IW, Kim TK, Kwon S, Lee JH, Lee J, Yu K. High-performance integrated perovskite and organic solar cells with enhanced fill factors and near-infrared harvesting. Adv Mater. 2016;28:3159.
[36] Elbohy H, Bahrami B, Mabrouk S, Reza KM, Gurung A, Pathak R, Liang M, Qiao Q, Zhu K. Tuning hole transport layer using urea for high-performance perovskite solar cells. Adv Funct Mater. 2019;29(47):1806740.
[37] Xiao K, Wen J, Han Q, Lin R, Gao Y, Gu S, Zang Y, Nie Y, Zhu J, Xu J. Solution-processed monolithic all-perovskite triple-junction solar cells with efficiency exceeding 20%. ACS Energy Lett. 2020;5(9):2819.
[38] Lin R, Xiao K, Qin Z, Han Q, Zhang C, Wei M, Saidaminov MI, Gao Y, Xu J, Xiao M. Monolithic all-perovskite tandem solar cells with 24.8% efficiency exploiting comproportionation to suppress Sn (II) oxidation in precursor ink. Nat Energy. 2019;4(10):864.
[39] Xiao K, Lin R, Han Q, Hou Y, Qin Z, Nguyen HT, Wen J, Wei M, Yeddu V, Saidaminov MI. All-perovskite tandem solar cells with 24.2% certified efficiency and area over 1 cm 2 using surface-anchoring zwitterionic antioxidant. Nat Energy. 2020;5(11):870.
[40] Ouyang J. "Secondary doping" methods to significantly enhance the conductivity of PEDOT: PSS for its application as transparent electrode of optoelectronic devices. Displays. 2013;34(5):423.
[41] Kim J, Jung J, Lee D, Joo J. Enhancement of electrical conductivity of poly (3, 4-ethylenedioxythiophene)/poly (4-styrenesulfonate) by a change of solvents. Synth Met. 2002;126(2–3):311.
[42] Alamer FA. A simple method for fabricating highly electrically conductive cotton fabric without metals or nanoparticles, using PEDOT: PSS. J. Alloys Compd. 2017;702(8):266.
[43] Ding Y, Invernale MA, Sotzing GA. Conductivity trends of PEDOT-PSS impregnated fabric and the effect of conductivity on electrochromic textile. ACS Appl Mater Interfaces. 2010;2(6):1588.
[44] Gomes L, Branco A, Moreira T, Feliciano F, Pinheiro C, Costa C. Increasing the electrical conductivity of electrochromic PEDOT: PSS films—a comparative study. Sol Energy Mater Sol Cells. 2016;144(10):631.
[45] Lee YY, Kang HY, Gwon SH, Choi GM, Lim SM, Sun JY, Joo YC. A strain-insensitive stretchable electronic conductor: PEDOT: PSS/acrylamide organogels. Adv Mater. 2016;28(8):1636.
[46] Ouyang J, Chu CW, Chen FC, Xu Q, Yang Y. High-conductivity poly (3, 4-ethylenedioxythiophene): poly (styrene sulfonate) film and its application in polymer optoelectronic devices. Adv Funct Mater. 2005;15(2):203.
[47] Vosgueritchian M, Lipomi DJ, Bao Z. Highly conductive and transparent PEDOT: PSS films with a fluorosurfactant for stretchable and flexible transparent electrodes. Adv Funct Mater. 2012;22(2):421.
[48] Xia Y, Sun K, Ouyang J. Solution-processed metallic conducting polymer films as transparent electrode of optoelectronic devices. Adv Mater. 2012;24(18):2436.
[49] Mengistie DA, Wang PC, Chu CW. Effect of molecular weight of additives on the conductivity of PEDOT: PSS and efficiency for ITO-free organic solar cells. J Mater Chem A. 2013;1(34):9907.
[50] Ouyang J, Xu Q, Chu CW, Yang Y, Li G, Shinar J. On the mechanism of conductivity enhancement in poly (3, 4 ethylenedioxythiophene): poly (styrene sulfonate) film through solvent treatment. Polymer. 2004;45(25):8443.
[51] Alemu D, Wei HY, Ho KC, Chu CW. Highly conductive PEDOT: PSS electrode by simple film treatment with methanol for ITO-free polymer solar cells. Energy Environ Sci. 2012;5(11):9662.
[52] Rivnay J, Inal S, Collins BA, Sessolo M, Stavrinidou E, Strakosas X, Tassone C, Delongchamp DM, Malliaras GG. Structural control of mixed ionic and electronic transport in conducting polymers. Nat Commun. 2016;7(1):1.
[53] Gelbwaser-Klimovsky D, Saikin SK, Goldsmith RH, Aspuru-Guzik A. Optical spectra of p-doped PEDOT nanoaggregates provide insight into the material disorder. ACS Energy Lett. 2016;1(6):1100.
[54] Reyes-Reyes M, Cruz-Cruz I, López-Sandoval R. Enhancement of the electrical conductivity in PEDOT: PSS films by the addition of dimethyl sulfate. J Phys Chem C. 2010;114(47):20220.

[55] Li Z, Liu C, Zhang X, Guo J, Cui H, Shen L, Bi Y, Guo W. Using easily prepared carbon nanodots to improve hole transport capacity of perovskite solar cells. Materials Today Energy. 2019;12(7):161.
[56] Stranks SD, Snaith HJ. Metal-halide perovskites for photovoltaic and light-emitting devices. Nat Nanotechnol. 2015; 10(5):391.
[57] Seo J, Park S, Kim YC, Jeon NJ, Noh JH, Yoon SC, Seok SI. Benefits of very thin PCBM and LiF layers for solution-processed p–i–n perovskite solar cells. Energy Environ Sci. 2014; 7(8):2642.
[58] Liu D, Li Y, Yuan J, Hong Q, Shi G, Yuan D, Wei J, Huang C, Tang J, Fung MK. Improved performance of inverted planar perovskite solar cells with F4-TCNQ doped PEDOT: PSS hole transport layers. J Mater Chem A. 2017;5(12):5701.
[59] Huang D, Goh T, Kong J, Zheng Y, Zhao S, Xu Z, Taylor AD. Perovskite solar cells with a DMSO-treated PEDOT: PSS hole transport layer exhibit higher photovoltaic performance and enhanced durability. Nanoscale. 2017;9(12):4236.
[60] Thomas JP, Zhao L, McGillivray D, Leung KT. High-efficiency hybrid solar cells by nanostructural modification in PEDOT: PSS with co-solvent addition. J Mater Chem A. 2014; 2(7):2383.
[61] Wang Y, Shao P, Chen Q, Li Y, Li J, He D. Nanostructural optimization of silicon/PEDOT: PSS hybrid solar cells for performance improvement. J Mater Chem A. 2017;50(17): 175105.
[62] Kim KM, Ahn S, Jang W, Park S, Park OO, Wang DH. Work function optimization of vacuum free top-electrode by PEDOT: PSS/PEI interaction for efficient semi-transparent perovskite solar cells. Sol Energy Mater Sol Cells. 2018;176(6):435.
[63] Xue Q, Liu M, Li Z, Yan L, Hu Z, Zhou J, Li W, Jiang XF, Xu B, Huang F. Efficient and stable perovskite solar cells via dual functionalization of dopamine semiquinone radical with improved trap passivation capabilities. Adv Funct Mater. 2018; 28(18):1707444.
[64] Dong H, Zheng E, Niu Z, Zhang X, Lin YY, Jain P, Yu Q. Hydroxymethyl-functionalized PEDOT-MeOH: PSS for perovskite solar cells. ACS Appl Mater Interfaces. 2020;12(15): 17571.
[65] Zhang M, Chi D, Wang J, Wu F, Huang S. Improved performance of lead-tin mixed perovskite solar cells with PEDOT: PSS treated by hydroquinone. Sol Energy. 2020;201:589.
[66] Zhao Z, Yuan L, Huang J, Shi J, Cao Y, Zi W, Zhang W. Modified HTL-induced efficiency enhancement for inverted perovskite solar cells. Org Electron. 2020;78:105557.
[67] Xu L, Li Y, Zhang C, Liu Y, Zheng C, Lv W, Li M, Chen Y, Huang W, Chen R. Improving the efficiency and stability of inverted perovskite solar cells by CuSCN-doped PEDOT: PSS. Sol Energy Mater Sol Cells. 2020;206(7):110316.
[68] Bao X, Wang J, Li Y, Zhu D, Wu Y, Guo P, Wang X, Zhang Y, Wang J, Yip HL. Interface engineering of a compatible PEDOT derivative bilayer for high-performance inverted perovskite solar cells. Adv Mater Interfaces. 2017;4(6):1600948.
[69] Hong N, Xiao J, Li Y, Li Y, Wu Y, Yu W, Qiu X, Chen R, Yip HL, Huang W. Unexpected fluorescent emission of graft sulfonated-acetone–formaldehyde lignin and its application as a dopant of PEDOT for high performance photovoltaic and light-emitting devices. J Mater Chem C. 2016;4(23):5297.
[70] Wu Y, Wang J, Qiu X, Yang R, Lou H, Bao X, Li Y. Highly efficient inverted perovskite solar cells with sulfonated lignin doped PEDOT as hole extract layer. ACS Appl Mater Interfaces. 2016;8(19):12377.
[71] Li Y, Liu T, Qiu X, Zhou Y, Li Y. Engineering enhancing efficiency and durability of inverted perovskite solar cells with phenol/unsaturated carbon–carbon double bond dual-functionalized poly (3, 4-ethylenedioxythiophene) hole extraction layer. ACS Sustain Chem Eng. 2018;7(1):961.
[72] Huang J, Wang C, Liu Z, Qiu X, Yang J, Chang J. Simultaneously enhanced durability and performance by employing dopamine copolymerized PEDOT with high work function and water-proofness for inverted perovskite solar cells. J Mater Chem C. 2018;6(9):2311.
[73] Yu W, Wang K, Guo B, Qiu X, Hao Y, Chang J, Li Y. Effect of ultraviolet absorptivity and waterproofness of poly (3, 4 ethylenedioxythiophene) with extremely weak acidity, high conductivity on enhanced stability of perovskite solar cells. J Power Sources. 2017;358(10):29.
[74] Yu W, Xie X, Li Y, Li Y, Chen R, Qiu X, Huang W. Poly (3, 4-ethylenedioxythiophene): sulfonated acetone-formaldehyde: preparation, characterization and performance as a hole injection material. J Mater Chem C. 2016;4(34):8077.
[75] Li Y, Liu M, Li Y, Yuan K, Xu L, Yu W, Chen R, Qiu X, Yip HL. Poly (3, 4-ethylenedioxythiophene): methylnaphthalene sulfonate formaldehyde condensate: the effect of work function and structural homogeneity on hole injection/extraction properties. Adv Energy Mater. 2017;7(6):1601499.
[76] Kim HS, Lee CR, Im JH, Lee KB, Moehl T, Marchioro A, Moon SJ, Humphry-Baker R, Yum JH, Moser JE. Lead iodide perovskite sensitized all-solid-state submicron thin film mesoscopic solar cell with efficiency exceeding 9%. Sci Rep. 2012; 2(1):1.
[77] Zhang H, Wu Y, Zhang W, Li E, Shen C, Jiang H, Tian H, Zhu WH. Low cost and stable quinoxaline-based hole-transporting materials with a D-A-D molecular configuration for efficient perovskite solar cells. Chem Sci. 2018;9(27):5919.
[78] Zhang F, Wang S, Zhu H, Liu X, Liu H, Li X, Xiao Y, Zakeeruddin SM, Grätzel M. Impact of peripheral groups on phenothiazine-based hole-transporting materials for perovskite solar cells. ACS Energy Lett. 2018;3(5):1145.
[79] Xu P, Liu P, Li Y, Xu B, Kloo L, Sun L, Hua Y. D–A–D-typed hole transport materials for efficient perovskite solar cells: tuning photovoltaic properties via the acceptor group. ACS Appl Mater Interfaces. 2018;10(23):19697.
[80] Zhang D, Xu P, Wu T, Ou Y, Yang X, Sun A, Cui B, Sun H, Hua Y. Cyclopenta[hi]aceanthrylene-based dopant-free hole-transport material for organic–inorganic hybrid and all-inorganic perovskite solar cells. J Mater Chem A. 2019; 7(10):5221.
[81] Wang Y, Chen W, Wang L, Tu B, Chen T, Liu B, Yang K, Koh CW, Zhang X, Sun H, Chen G, Feng X, Han YW, Aleksandra BD, He Z, Guo X. Dopant-free small-molecule hole-transporting material for inverted perovskite solar cells with efficiency exceeding 21%. Adv Mater. 2019;31(35):1902781.
[82] Pham HD, Jain SM, Li M, Wang ZK, Manzhos S, Feron K, Pitchaimuthu S, Liu Z, Motta N, Durrant JR. Molecular engineering using an anthanthrone dye for low-cost hole transport materials: a strategy for dopant-free, high-efficiency, and stable perovskite solar cells. Adv Energy Mater. 2018;8(16): 1703007.
[83] Pham HD, Jain SM, Li M, Wang ZK, Manzhos S, Feron K, Pitchaimuthu S, Liu Z, Motta N, Durrant JR. All-rounder low-cost dopant-free D-A-D hole-transporting materials for efficient indoor and outdoor performance of perovskite solar cells. Adv Electron Mater. 2020;6(4):1900884.
[84] Yin X, Zhou J, Song Z, Dong Z, Bao Q, Shrestha N, Bista SS, Ellingson RJ, Yan Y, Tang W. Dithieno [3, 2-b: 2′, 3-d] pyrrol-cored hole transport material enabling over 21% efficiency dopant-free perovskite solar cells. Adv Funct Mater. 2019; 29(38):1904300.
[85] Cao Y, Li Y, Morrissey T, Lam B, Patrick BO, Dvorak DJ, Xia Z, Kelly TL, Berlinguette CP. Dopant-free molecular hole

transport material that mediates a 20% power conversion efficiency in a perovskite solar cell. Energy Environ Sci. 2019; 12(12):3502.
[86] Jiang K, Wang J, Wu F, Xue Q, Yao Q, Zhang J, Chen Y, Zhang G, Zhu Z, Yan H, Zhu L, Yip HL. Dopant-free organic hole-transporting material for efficient and stable inverted all-inorganic and hybrid perovskite solar cells. Adv Mater. 2020;32(16):1908011.
[87] Zheng A, Ren M, Zhang Y, Cai Y, Zhang J, Yuan Y, Lei M, Wang P. A thioxanthenothioxanthene-based hole transporter with 2D molecular stacking for efficient and thermostable perovskite solar cells. ACS Mater Lett. 2020;2(7):691.
[88] Dong Y, Zhu H, Cao X, Han YP, Zhang HY, Yang Q, Zhang Y, Zhao J, Yin G, Wang S. Simple 9, 10-dihydrophenanthrene based hole-transporting materials for efficient perovskite solar cells. Chem Eng J. 2020;402(1):126298.
[89] Xue Y, Wu Y, Li Y. Readily synthesized dopant-free hole transport materials with phenol core for stabilized mixed perovskite solar cells. J Power Sources. 2017;344(10):160.
[90] Liu D, Kelly TL. Perovskite solar cells with a planar heterojunction structure prepared using room-temperature solution processing techniques. Nat Photonics. 2014;8(2):133.
[91] Zhu Z, Bai Y, Liu X, Chueh CC, Yang S, Jen AKY. Enhanced efficiency and stability of inverted perovskite solar cells using highly crystalline SnO_2 nanocrystals as the robust electron-transporting layer. Adv Mater. 2016;28(30):6478.
[92] Tiong V, Pham ND, Wang T, Zhu T, Zhao X, Zhang Y, Shen Q, Bell J, Hu L, Dai S. Octadecylamine-functionalized single-walled carbon nanotubes for facilitating the formation of a monolithic perovskite layer and stable solar cells. Adv Funct Mater. 2018;28(10):1705545.
[93] Kim HS, Lee JW, Yantara N, Boix PP, Kulkarni SA, Mhaisalkar S, Grätzel M, Park NG. High efficiency solid-state sensitized solar cell-based on submicrometer rutile TiO_2 nanorod and $CH_3NH_3PbI_3$ perovskite sensitizer. Nano Lett. 2013;13(6):2412.
[94] Zardetto V, Williams B, Perrotta A, Di Giacomo F, Verheijen M, Andriessen R, Kessels W, Creatore M. Atomic layer deposition for perovskite solar cells: research status, opportunities and challenges. Sustain Energy Fuels. 2017;1(1):30.
[95] Yang D, Yang R, Zhang J, Yang Z, Liu SF, Li C. High efficiency flexible perovskite solar cells using superior low temperature TiO_2. Energy Environ Sci. 2015;8(11):3208.
[96] Wang K, Shi Y, Dong Q, Li Y, Wang S, Yu X, Wu M, Ma T. Low-temperature and solution-processed amorphous WO_X as electron-selective layer for perovskite solar cells. J Phys Chem Lett. 2015;6(5):755.
[97] Agresti A, Pescetelli S, Palma AL, Castillo AEDR, Konios D, Kakavelakis G, Razza S, Cinà L, Kymakis E, Bonaccorso F. Graphene interface engineering for perovskite solar module: a power conversion efficiency exceeding 12.5% over 50 cm^2 active area. ACS Energy Lett. 2017;2(1):279.
[98] Ahn N, Kwak K, Jang MS, Yoon H, Lee BY, Lee JK, Pikhitsa PV, Byun J, Choi M. Trapped charge-driven degradation of perovskite solar cells. Nat Commun. 2016;7(1):1.
[99] Grätzel M. The light and shade of perovskite solar cells. Nat Mater. 2014;13(9):838.
[100] Yella A, Heiniger LP, Gao P, Nazeeruddin MK, Grätzel M. Nanocrystalline rutile electron extraction layer enables low-temperature solution processed perovskite photovoltaics with 13.7% efficiency. Nano Lett. 2014;14(5):2591.
[101] Wang J, Ball JM, Barea EM, Abate A, Alexander-Webber JA, Huang J, Saliba M, Mora-Sero I, Bisquert J, Snaith H, Nicholas RJ. Low-temperature processed electron collection layers of graphene/TiO_2 nanocomposites in thin film perovskite solar cells. Nano Lett. 2014;14(2):724.
[102] Zhou Q, Du J, Duan J, Wang Y, Yang X, Duan Y, Tang Q. Photoactivated transition metal dichalcogenides to boost electron extraction for all-inorganic tri-brominated planar perovskite solar cells. J Mater Chem A. 2020;8(16):7784.
[103] Ball JM, Lee MM, Hey A, Snaith H. Low-temperature processed meso-superstructured to thin-film perovskite solar cells. Energy Environ Sci. 2013;6(6):1739.
[104] Wang Q, Shao Y, Dong Q, Xiao Z, Yuan Y, Huang J. Large fill-factor bilayer iodine perovskite solar cells fabricated by a low-temperature solution-process. Energy Environ Sci. 2014; 7(7):2359.
[105] Cai Q, Zhang Y, Liang C, Li P, Gu H, Liu X, Wang J, Shentu Z, Fan J, Shao G. Enhancing efficiency of planar structure perovskite solar cells using Sn-doped TiO_2 as electron transport layer at low temperature. Electrochim Acta. 2018;261(9):227.
[106] Liao YH, Chang YH, Lin TH, Chan SH, Lee KM, Hsu KH, Hsu JF, Wu MC. Boosting the power conversion efficiency of perovskite solar cells based on Sn doped TiO_2 electron extraction layer via modification the TiO_2 phase junction. Sol Energy. 2020;205:390.
[107] Yin G, Ma J, Jiang H, Li J, Yang D, Gao F, Zeng J, Liu Z, Liu SF. Enhancing efficiency and stability of perovskite solar cells through Nb-doping of TiO_2 at low temperature. ACS Appl Mater Interfaces. 2017;9(12):10752.
[108] Sanehira Y, Shibayama N, Numata Y, Ikegami M, Miyasaka T. Low-temperature synthesized Nb-doped TiO_2 electron transport layer enabling high-efficiency perovskite solar cells by band alignment tuning. ACS Appl Mater Interfaces. 2020; 12(13):15175.
[109] Kim JY, Rhee S, Lee H, An K, Biswas S, Lee Y, Shim JW, Lee C, Kim H. Universal elaboration of Al-doped TiO_2 as an electron extraction layer in inorganic–organic hybrid perovskite and organic solar cells. Adv Mater Interfaces. 2020; 7(10):1902003.
[110] Xu Z, Yin X, Guo Y, Pu Y, He M. Ru-doping in TiO_2 electron transport layers of planar heterojunction perovskite solar cells for enhanced performance. J Mater Chem C. 2018;6(17):4746.
[111] Liu X, Liu Z, Sun B, Tan X, Ye H, Tu Y, Shi T, Tang Z, Liao G. 17.46% efficient and highly stable carbon-based planar perovskite solar cells employing Ni-doped rutile TiO_2 as electron transport layer. Nano Energy. 2018;50(11):201.
[112] Halvani AE, Kermanpur A, Mayer MT, Steier L, Ahmed T, Turren-Cruz SH, Seo J, Luo J, Zakeeruddin SM, Tress WR. Low-temperature Nb-doped SnO_2 electron-selective contact yields over 20% efficiency in planar perovskite solar cells. ACS Energy Lett. 2018;3(4):773.
[113] Wang Y, Wan J, Ding J, Hu JS, Wang D. A rutile TiO_2 electron transport layer for the enhancement of charge collection for efficient perovskite solar cells. Angew Chem Int Ed. 2019; 58(28):9414.
[114] Liu Z, Chen Q, Hong Z, Zhou H, Xu X, De Marco N, Sun P, Zhao Z, Cheng YB, Yang Y. Low-temperature TiO_x compact layer for planar heterojunction perovskite solar cells. ACS Appl Mater Interfaces. 2016;8(17):11076.
[115] Shahvaranfard F, Altomare M, Hou Y, Hejazi S, Meng W, Osuagwu B, Li N, Brabec CJ, Schmuki P. Engineering of the electron transport layer/perovskite interface in solar cells designed on TiO_2 rutile nanorods. Adv Funct Mater. 2020; 30(10):1909738.
[116] Zhang Y, Liu X, Li P, Duan Y, Hu X, Li F, Song Y. Dopamine-crosslinked TiO_2/perovskite layer for efficient and photostable perovskite solar cells under full spectral continuous illumination. Nano Energy. 2019;56(8):733.
[117] Liu Z, Deng K, Hu J, Li L. Coagulated SnO_2 colloids for high-performance planar perovskite solar cells with negligible

hysteresis and improved stability. Angew Chem. 2019;131(33): 11621.
[118] Chen J, Zhao X, Kim SG, Park NG. Multifunctional chemical linker imidazoleacetic acid hydrochloride for 21% efficient and stable planar perovskite solar cells. Adv Mater. 2019;31(39): 1902902.
[119] Shao Y, Xiao Z, Bi C, Yuan Y, Huang J. Origin and elimination of photocurrent hysteresis by fullerene passivation in $CH_3NH_3PbI_3$ planar heterojunction solar cells. Nat Commun. 2014;5(1):1.
[120] Ueno H, Jeon I, Lin HS, Thote A, Nakagawa T, Okada H, Izawa S, Hiramoto M, Daiguji H, Maruyama S, Matsuo Y. Li@C_{60} endohedral fullerene as a supraatomic dopant for C60 electron-transporting layers promoting the efficiency of perovskite solar cells. Chem Commun. 2019;55(79):11837.
[121] Wang YC, Chang J, Zhu L, Li X, Song C, Fang J. Electron-transport-layer-assisted crystallization of perovskite films for high-efficiency planar heterojunction solar cells. Adv Funct Mater. 2018;28(9):1706317.
[122] Ranjan R, Usmani B, Pali S, Ranjan S, Singh A, Garg A, Gupta RK. Role of $PC_{60}BM$ in defect passivation and improving degradation behaviour in planar perovskite solar cells. Sol Energy Mater Sol Cells. 2020;207(1):110335.
[123] Li D, Kong W, Zhang H, Wang D, Li W, Liu C, Chen H, Song W, Gao F, Amini A, Xu B, Li S, Cheng C. Bifunctional ultrathin PCBM enables passivated trap states and cascaded energy level toward efficient inverted perovskite solar cells. ACS Appl Mater Interfaces. 2020;12(17):20103.
[124] Chen C, Zhang S, Wu S, Zhang W, Zhu H, Xiong Z, Zhang Y, Chen W. Effect of BCP buffer layer on eliminating charge accumulation for high performance of inverted perovskite solar cells. RSC Adv. 2017;7(57):35819.
[125] Yang Q, Dettori R, Achenie L. A perovskite solar cell with enhanced light stability and high photovoltaic conversion efficiencies. ACS Sustain Chem Eng. 2018;7(1):709.
[126] Liu X, Li X, Zou Y, Liu H, Wang L, Fang J, Yang C. Energy level-modulated non-fullerene small molecule acceptors for improved V_{OC} and efficiency of inverted perovskite solar cells. J Mater Chem A. 2019;7(7):3336.
[127] Hu Z, Tang G, Miao J, Fu T, Li T, Tai Q, Meng H, Yan F. π-extended Spiro core-based nonfullerene electron-transporting material for high-performance perovskite solar cells. Adv Funct Mater. 2020;30(25):2001073.
[128] Miao J, Hu Z, Liu M, Ali MU, Goto O, Lu W, Yang T, Liang Y, Meng H. A non-fullerene small molecule processed with green solvent as an electron transporting material for high efficiency p-i-n perovskite solar cells. Org Electron. 2017; 52(6):200.
[129] Jiang K, Wu F, Yu H, Yao YQ, Zhang GY, Zhu LN, Yan H. A perylene diimide-based electron transport layer enabling efficient inverted perovskite solar cells. J Mater Chem A. 2018; 6(35):16868.
[130] Singh A, Chen HC, Chen YF, Lu YJ, Wong KT, Chu CW. Core-twisted tetrachloroperylenediimides: low-cost and efficient non-fullerene organic electron-transporting materials for inverted planar perovskite solar cells. Chemsuschem. 2020; 13(14):3686.
[131] Luo J, Li X, Chen J, Huang F, Cao Y. Efficient three-color white light-emitting diodes from a single polymer with PFN/Al bilayer cathode. Synth Met. 2011;161(17–18):1982.
[132] Zhang K, Zhong C, Liu S, Liang A-H, Dong S, Huang F. High efficiency solution processed inverted white organic light emitting diodes with a cross-linkable amino-functionalized polyfluorene as a cathode interlayer. J Mater Chem C. 2014; 2(17):3270.
[133] Peng Z, Zhang Y, Xia Y, Xiong K, Cai C, Xia L, Hu Z, Zhang K, Huang F, Hou L. One-step coating inverted polymer solar cells using a conjugated polymer as an electron extraction additive. J Mater Chem A. 2015;3(41):20500.
[134] Wang C, Luo Y, Zheng J, Liu L, Xie Z, Huang F, Yang B, Ma Y. Spontaneous interfacial dipole orientation effect of acetic acid solubilized PFN. ACS Appl Mater Interfaces. 2018; 10(12):10270.
[135] Li D, Sun C, Li H, Shi H, Shai X, Sun Q, Han J, Shen Y, Yip HL, Huang F. Amino-functionalized conjugated polymer electron transport layers enhance the UV-photostability of planar heterojunction perovskite solar cells. Chem Sci. 2017; 8(6):4587.
[136] Sun C, Wu Z, Yip HL, Zhang H, Jiang XF, Xue Q, Hu Z, Hu Z, Shen Y, Wang M. Amino-functionalized conjugated polymer as an efficient electron transport layer for high-performance planar-heterojunction perovskite solar cells. Adv Energy Mater. 2016;6(5):1501534.
[137] Wang J, Lin K, Zhang K, Jiang XF, Mahmood K, Ying L, Huang F, Cao Y. Crosslinkable amino-functionalized conjugated polymer as cathode interlayer for efficient inverted polymer solar cells. Adv Energy Mater. 2016;6(11):1502563.
[138] Zhu L, Song C, Li X, Wang YC, Zhang W, Sun X, Zhang W, Fang J. A benzobis (thiadiazole)-based small molecule as a solution-processing electron extraction material in planar perovskite solar cells. J Mater Chem C. 2017;5(41):10777.
[139] Wan L, Li X, Song C, He Y, Zhang W. Benzobis (thiadiazole)-based small molecules as efficient electron transporting materials in perovskite solar cells. Sol Energy Mater Sol Cells. 2019;191(7):437.
[140] Li H, Zhang W. Perovskite tandem solar cells: from fundamentals to commercial deployment. Chem Rev. 2020;120(18): 9835.
[141] Jeong M, Choi IW, Go EM, Cho Y, Kim M, Lee B, Jeong S, Jo Y, Choi HW, Lee J, Bae JH, Kwak SK, Kim DS, Yang C. Stable perovskite solar cells with efficiency exceeding 24.8% and 0.3-V voltage loss. Science. 2020;369(6511):1615.
[142] Lian J, Lu B, Niu F, Zeng P, Zhan X. Electron-transport materials in perovskite solar cells. Small Methods. 2018;2(10): 1800082.
[143] Mao GP, Wang W, Shao S, Sun XJ, Chen SA, Li MH, Li HM. Research progress in electron transport layer in perovskite solar cells. Rare Met. 2018;37(1): 5.
[144] Haider M, Yang JL. Efficient and stable perovskite–silicon two-terminal tandem solar cells. Rare Met. 2020;39(7):745.
[145] Huang T, Liu H, Bang Y, Wang Y, Liang Y, Wang X, Zhang Y, Xie S, Zeng Z, Tang BZ. Spiro-conjugated indenodiarylethenes: enabling steric-induced electronic tuning of photochromic and photoluminescent properties by spiro-conjugation. Sci China Chem. 2020;63(11):1659.
[146] Zhou Z, Xie S, Chen X, Tu Y, Xiang J, Wang J, He Z, Zeng Z, Tang BZ. Spiro-functionalized diphenylethenes: suppression of a reversible photocyclization contributes to the aggregation-induced emission effect. J Am Chem Soc. 2019;141(25): 9803.
[147] Fagiolari L, Bella F. Carbon-based materials for stable, cheaper and large-scale processable perovskite solar cells. Energy Environ Sci. 2019;12(12):3437.
[148] Zhou J, Zhu W, Zeng M, Yang Q, Li P, Lan L, Peng J, Li Y, Fei H, Cao Y. Aromatic inorganic acid radical. Sci China Chem. 2019;62(12):1656.

Yuan Li received Ph.D. degree from South China University of Technology in 2010. From 2010 to 2013, he conducted postdoctoral research in National University of Singapore and he started the independent research work from 2013 in South China University of Technology as associate professor. He published more than 60 peer-reviewed scientific papers, and the main research interests are focused on design of novel and stable organic radical semiconductors, as well as their applications in perovskite solar cells and organic electronic devices.